

Late Cretaceous blueschist facies metamorphism in southern Thrace (Turkey) and its geodynamic implications

G. TOPUZ,¹ A. I. OKAY,¹ R. ALTHERR,² M. SATIR³ AND W. H. SCHWARZ²

¹Eurasian Institute of Earth Sciences, Technical University of Istanbul, Ayazağa 80626, Istanbul, Turkey (topuzg@itu.edu.tr)

²Institute of Mineralogy, University of Heidelberg, Im Neuenheimer Feld 236, D-69120 Heidelberg, Germany

³Institute of Geosciences (Geochemistry), University of Tübingen, Wilhelmstrasse 56, D-72074 Tübingen, Germany

ABSTRACT A blueschist facies tectonic sliver, 9 km long and 1 km wide, crops out within the Miocene clastic rocks bounded by the strands of the North Anatolian Fault zone in southern Thrace, NW Turkey. Two types of blueschist facies rock assemblages occur in the sliver: (i) A serpentinite body with numerous dykes of incipient blueschist facies metadiabase (ii) a well-foliated and thoroughly recrystallized rock assemblage consisting of blueschist, marble and metachert. Both are partially enveloped by an Upper Eocene wildflysch, which includes olistoliths of serpentinite–metadiabase, Upper Cretaceous and Palaeogene pelagic limestone, Upper Eocene reefal limestone, radiolarian chert, quartzite and minor greenschist. Field relations in combination with the bore core data suggest that the tectonic sliver forms a positive flower structure within the Miocene clastic rocks in a transpressional strike–slip setting, and represents an uplifted part of the pre-Eocene basement. The blueschists are represented by lawsonite–glaucophane-bearing assemblages equilibrated at 270–310 °C and ~0.8 GPa. The metadiabase dykes in the serpentinite, on the other hand, are represented by pumpellyite–glaucophane–lawsonite-assemblages that most probably equilibrated below 290 °C and at 0.75 GPa. One metadiabase olistolith in the Upper Eocene flysch sequence contains the mineral assemblage epidote + pumpellyite + glaucophane, recording *P–T* conditions of 290–350 °C and 0.65–0.78 GPa, indicative of slightly lower depths and different thermal setting. Timing of the blueschist facies metamorphism is constrained to *c.* 86 Ma (Coniacian/Santonian) by Rb–Sr phengite–whole rock and incremental ⁴⁰Ar–³⁹Ar phengite dating on blueschists. The activity of the strike–slip fault post-dates the blueschist facies metamorphism and exhumation, and is only responsible for the present outcrop pattern and post-Miocene exhumation (~2 km). The high-*P/T* metamorphic rocks of southern Thrace and the Biga Peninsula are located to the southeast of the Circum Rhodope Belt and indicate Late Cretaceous subduction and accretion under the northern continent, i.e. the Rhodope Massif, enveloped by the Circum Rhodope Belt. The Late Cretaceous is therefore a time of continued accretionary growth of this continental domain.

Key words: accretionary complex; blueschist facies metamorphism; olistolith; Rb–Sr and ⁴⁰Ar–³⁹Ar dating; Rhodopes; Thrace; Turkey.

INTRODUCTION

Blueschist facies rocks, low-temperature eclogites and accretionary complexes are principal markers of former subduction zones and are formed during oceanic subduction preceding the terminal continental collision (e.g. Maruyama *et al.*, 1996). Exhumation and outcrop patterns of these rocks are fundamentally determined by tectonic events: They occur in fault-bounded elongate units, which may represent (i) a coherent sequence formed at nearly the same depth in a subduction channel (e.g. Goodge, 1995; Okay *et al.*, 1998); (ii) a mélange with matrix and blocks of similar metamorphic ages, but reflecting a diverse range of *P–T* conditions (e.g. Goodge & Renne, 1993; Goodge, 1995; Spaggiari *et al.*, 2002; Davis & Whitney, 2006, 2008) or (iii) a metamorphic sequence with older high-grade exotic tectonic blocks (e.g. Moore, 1984; Wakabayashi, 1990; Anczkiewicz *et al.*, 2004; Tsujimori *et al.*,

2006). Later tectonic and sedimentary events can modify the outcrop patterns and transfer the high-*P/T* rocks as olistoliths into a new sedimentation milieu. Therefore, a combination of petrological and geochronological data together with field geological constraints is crucial to trace the evolution of rock types formed in subduction zones.

In southern Thrace, a blueschist facies tectonic sliver, 9 km long and 1 km wide, crops out bounded by subsidiary strands of the North Anatolian Fault (Figs 1 & 2). In the vicinity (~100 km), there is no other known exposure of comparable blueschist facies lithologies. This paper deals with the field relations, petrology and age of these blueschist facies lithologies and discusses these data in terms of their origin and emplacement. The results suggest that the blueschist facies rocks were derived from an oceanic accretionary complex of Late Cretaceous age, and represent an uplifted sliver of the pre-Eocene basement of southern

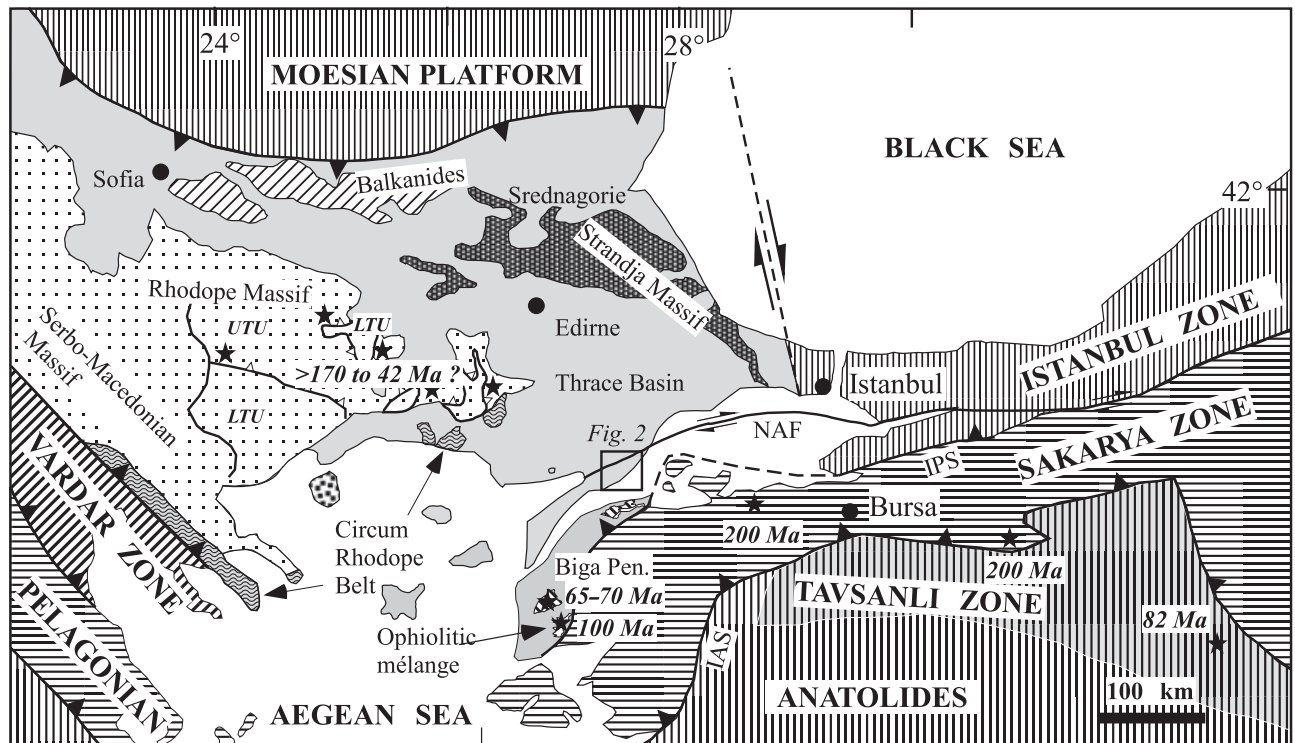


Fig. 1. Main tectonic units of the northern Aegean, the Balkanides and NW Turkey (modified from Okay & Satir, 2000a). Asterisks mark the location of eclogite occurrences, the numbers in Ma designate their ages. LTU, lower tectonic unit; UTU, upper tectonic unit of Rhodore Massif; NAF, North Anatolian Fault; IPS, intra-Pontide suture; IAS, Izmir-Ankara suture. Thick lines with solid triangles indicate sutures with subduction polarities, that with open triangles major thrusts.

Thrace. Together with the wide exposures of Late Cretaceous high-pressure metamorphic micaschists and eclogites as well as non-metamorphic accretionary complexes in the NW Biga peninsula, these rocks indicate substantial accretionary crustal growth during late Cretaceous time.

GEOLOGICAL SETTING AND FIELD RELATIONS

Thrace, the European part of Turkey, is the site of a Tertiary clastic basin with a >6-km-thick Middle Eocene to Upper Oligocene sequence of sandstone, siltstone and shale (Fig. 1). This Eocene–Oligocene series is unconformably overlain by a Miocene sequence of fluvial to lagoonal rocks (e.g. Kopp *et al.*, 1969; Turgut *et al.*, 1991; Görür & Okay, 1996). In the northeast and southwest, the basement of this Tertiary basin is represented by metamorphic rocks of the Strandja and Rhodore Massifs respectively. The Strandja Massif has a Variscan crystalline basement, intruded by early Permian granites and unconformably overlain by Triassic to Jurassic epicontinental sedimentary rocks (Okay *et al.*, 2001; Sunal *et al.*, 2006). It underwent a second phase of north-vergent deformation and metamorphism during the latest Jurassic, and the metamorphic rocks are unconformably overlain by Cenomanian sandstones and limestones.

The Rhodore Massif, on the other hand, comprises a nappe stack, differentiated essentially into two tectonic units (e.g. Burg *et al.*, 1996; Ricou *et al.*, 1998; van Hinsbergen *et al.*, 2005): (i) a lower tectonic unit consisting of orthogneiss, pelitic gneiss and schist with local intercalations of eclogitic amphibolite and (ii) an upper tectonic unit comprising interlayered amphibolites, marbles, metapelitic schists and various gneisses enclosing eclogite and metaperidotite lenses. The upper tectonic unit underwent high-*T* eclogite to ultrahigh-pressure metamorphism, followed by an amphibolite to granulite facies overprint, whereas the lower tectonic unit underwent low-*T* eclogite facies metamorphism that was overprinted by lower amphibolite to upper greenschist facies metamorphism (e.g. Liati & Mposkos, 1990; Liati & Seidel, 1996; Liati & Gebauer, 1999; Mposkos & Kostopoulos, 2001; Liati *et al.*, 2002; Liati, 2005). The timings of metamorphic and deformational events are poorly known, with isotopic ages ranging from Late Jurassic to Eocene (Liati, 2005; Bonev *et al.*, 2006; Mposkos & Krohe, 2006; Bauer *et al.*, 2007). Rock units combined under the term Circum-Rhodore Belt form an allochthonous ‘envelope’ along the southeastern border of the Rhodore Massif and comprise Triassic to Early Cretaceous neritic to pelagic sediments (Kauffmann *et al.*, 1976), associated with greenschist facies (Maganas *et al.*,

1991; Magganas, 2002; Bonev & Stampfli, 2003, 2008) and low-grade high-*P*/low-*T* metamorphic rocks (Michard *et al.*, 1994).

The metamorphic rocks of the Rhodope Massif and the overlying Tertiary sedimentary sequences are locally crosscut by late Eocene to late Oligocene calcalkaline and late Miocene alkaline volcanic rocks that occur throughout Thrace (e.g. Ercan, 1992; Aldanmaz *et al.*, 2006). Upper Cretaceous volcano-sedimentary rocks and granodioritic plutons are confined to the Strandja Massif and the areas farther north (Fig. 1).

The seismically active Ganos right-lateral strike-slip fault, which forms the western extension of the North Anatolian Fault in Thrace, cuts and deforms the sediments of the Thrace basin. An elongate ridge of blueschist facies rocks, ~9 km long and 1 km wide, and unconformably overlain by Upper Eocene shallow marine limestones, crops out in the Ganos fault zone northwest of Şarköy. This Sarıkaya blueschist facies sliver forms a positive flower structure and is thrust bilaterally over Miocene sandstones (Figs 2 & 3; Okay *et al.*, 1999). In the east, the sliver is in tectonic contact with an olistostromal Upper Eocene turbidite sequence. The Upper Eocene series form a sandstone–shale sequence with horizons of debris flows and olistostromes. The olistoliths are Upper Eocene neritic limestone, Upper Cretaceous and Palaeogene pelagic limestone, serpentinite + metadiabase, radiolarian

chert, quartzite and rare greenschist (Okay & Tansel, 1992; this study). They range up to several hundreds of metres in size; some of the blocks are composite, consisting of basalt or pelagic limestone unconformably overlain by shallow marine Upper Eocene limestone.

The Sarıkaya blueschist facies sliver could represent either a very large olistolith in the Upper Eocene sequence or an uplifted segment of the basement. The Ortaköy-1 petroleum exploration well south of the Sarıkaya ridge has cut through the Miocene series, the olistostromal Eocene sequence and the Upper Eocene limestones, and reached a basement of serpentinite at a depth of 1731 m (Figs 2 & 4). The results from this well suggest that the Sarıkaya blueschist facies sliver probably represents an uplifted segment of the basement.

The Sarıkaya blueschist facies sliver comprises a large serpentinite body and a well-foliated block of blueschist, marble and metachert (Figs 2 & 3). The serpentinite body, 9 km by 1 km, predominantly consists of dark green serpentinite (~90 % of the outcrop area) including abundant greenish grey, up to 20-m thick, metadiabase bodies (~10%), and local pink to yellowish metarodingite veins, up to 1-m thick. Serpentinite is highly fractured and sheared or massive. Both the metadiabase and metarodingite bodies are free of penetrative foliation, and have sharp, generally

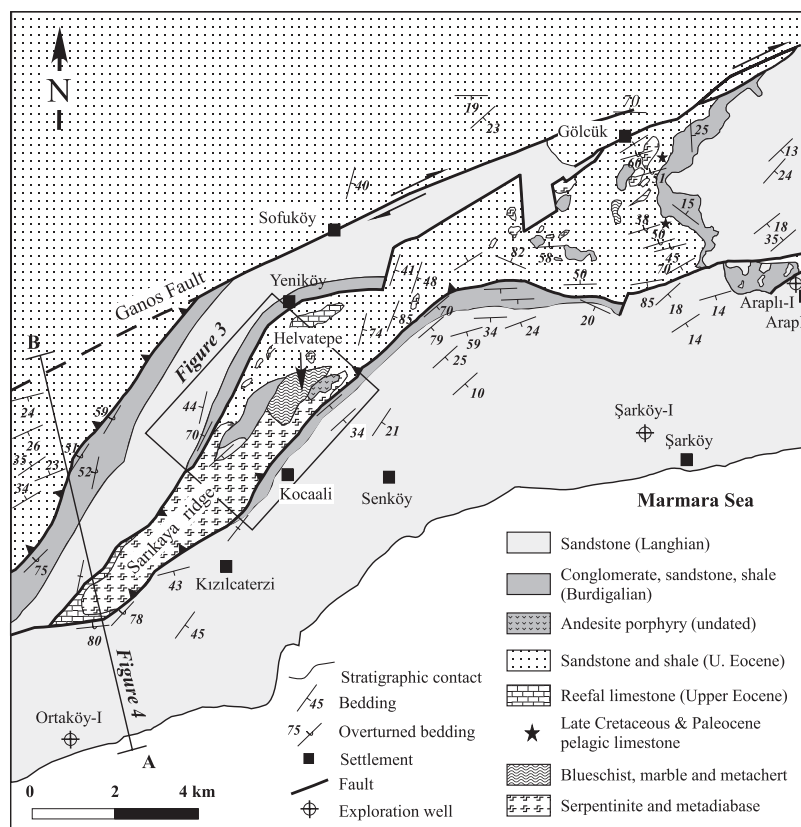


Fig. 2. Geological map of the Şarköy area. For location see Fig. 1.

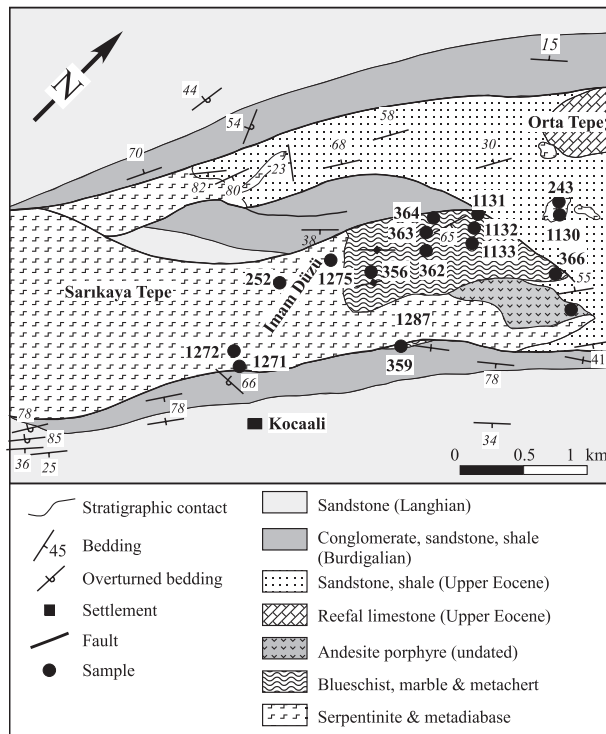


Fig. 3. Detailed geological map of the blueschist body showing the sample locations. For location see Fig. 2.

sheared contacts with the host serpentinite. Chilled margins in some metadiabase bodies indicate that they represent dykes rather than tectonic blocks. However, because of the subsequent deformation, the metadiabase dykes cannot be traced along strike for more than 100 m. The metadiabases are fine- to medium-grained, massive and very hard. Because of their hardness and homogenous texture, they were used as stone tools in pre-historic times (Özbek & Erol, 2001).

The well-foliated block of blueschist, marble and metachert, 2 km by 0.7 km, occurs in the vicinity of

the Helvatepe (Figs 2 & 3), and is in tectonic contact with serpentinite and Upper Eocene flysch (sandstone and shale). Within the block, blueschist represents the dominant rock type, while metachert and marble are subordinate. In contrast to the serpentinite body, no metadiabase dykes are present within the Helvatepe block. In the NE part of the study area, the blueschist facies sliver is in contact with a small andesitic intrusion and with the Upper Eocene sandstones and shales that contain several olistoliths of serpentinite and metadiabase (samples 243 & 1130; Figs 2 & 4).

PETROGRAPHY

Metadiabase rocks within serpentinite contain incipient blueschist facies mineral assemblages, and display a homogeneous intergranular texture. Primary magmatic textures are more or less preserved along with magmatic clinopyroxene, hornblende and ilmenite. Within some igneous clinopyroxenes, a core and an overgrowth domain can be differentiated (Fig. 5a). The boundary between the core and overgrowth is sharp. Magmatic hornblende usually overgrows clinopyroxene or replaces it along its fractures, indicating late-stage magmatic hydrothermal reactions (Fig. 5a,b). Metamorphic minerals occur in randomly oriented patches, implying that the metamorphism was not associated with penetrative deformation (Fig. 5b–f). The incomplete replacement of the magmatic clinopyroxene and hornblende, patchy nature of the metamorphic minerals and obvious dependence of the metamorphic minerals on the precursor ones suggest that the equilibrium is at best reached at very local scales, e.g. at the scales of the grain size.

Relict igneous clinopyroxene and hornblende are irregularly replaced by actinolite + glaucophane + phengite ± titanite ± chlorite (Fig. 5a,b), whereas plagioclase is transformed to fine-grained aggregates of pumpellyite + lawsonite + phengite + albite or epidote ± sodic pyroxene and ± quartz (Fig. 5c,d). Actinolite and glaucophane show no obvious

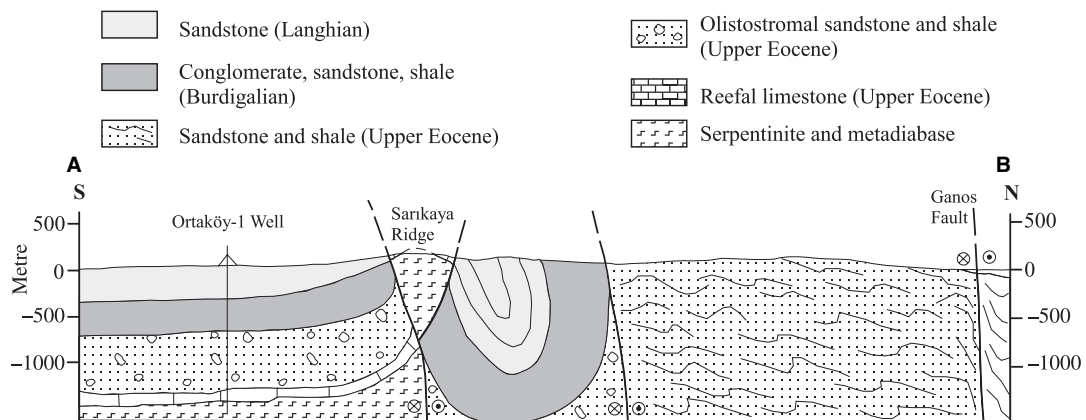


Fig. 4. North-south geological cross-section of the Sarköy area. For the location of the section, see Fig. 2.

replacement relationship, suggesting that they are mutually stable. Coexisting sodic and calcic amphiboles have frequently been described from blueschist facies rocks (e.g. Himmelberg & Papike, 1969; Ernst, 1979; Liou & Maruyama, 1987; Krogh *et al.*, 1994). This coexistence can be explained by a miscibility gap between sodic and calcic amphiboles, closing at temperatures ~ 600 °C (e.g. Reynard & Ballèvre, 1988). Sodic pyroxene forms fine to patchy or spongy grains intergrown with albite and phengite (Fig. 5d,f). Titanite contains patchy, partially resorbed inclusions of ilmenite \pm rutile.

Two varieties of metadiabase are distinguished on the basis of the Ca–Al mineral association and the occurrence of minor garnet and biotite (Table 1): (type I) pumpellyite + lawsonite, and (type II) pumpellyite + epidote + garnet + biotite (Fig. 5c,d). Type-I metadiabase bodies (samples 252 & 1275) occur in the Sarikaya serpentinite body, and type-II metadiabase (243, 1130A) occurs as olistolith within the Eocene sandstones and shales (Fig. 4). Biotite forms up to ~ 15 - μm -thick seams adjacent to phengite and pumpellyite (Fig. 5d). Garnet is found as small euhedral grains (~ 50 μm) in contact with pumpellyite, phengite and albite (Fig. 5e).

Blueschists are generally fine-grained and are more thoroughly recrystallized than the metadiabases. The main metamorphic assemblage is glaucophane–magnesioriebeckite + lawsonite \pm actinolite \pm sodic pyroxene + quartz + phengite + titanite + albite \pm chlorite (Table 1). These mineral assemblages are indicative of the lawsonite–blueschist subfacies (Evans, 1990). Primary igneous textures are locally recognizable in the form of relict clinopyroxenes and pseudomorphs consisting of lawsonite + quartz \pm albite \pm chlorite after former plagioclase phenocrysts (Fig. 6a–c). Relict igneous clinopyroxene is irregularly replaced or overgrown by sodic pyroxene together with sodic amphibole, lawsonite and titanite along cracks (Fig. 6a,b), similar to the pseudomorphs described by Okay (1982) and Maruyama & Liou (1985). Sodic pyroxene is locally replaced by a second generation of jadeite-poor sodic pyroxene and albite. Lawsonite and sodic amphibole form up to 300- μm -long idioblastic grains with local minute inclusions of quartz (Fig. 6d–e). Epidote occurs sporadically in some samples overgrowing glaucophane–magnesioriebeckite (Fig. 6e).

Carbonate-rich blueschists are composed of calcite + phengite + glaucophane–magnesioriebeckite + lawsonite + actinolite + chlorite + albite \pm sodic pyroxene + titanite + quartz (Table 1). They differ from the blueschists *sensu stricto* by the high amounts of calcite and phengite, and are probably derived from volcanoclastic material. No relict minerals and textures are preserved. Sodic pyroxene occurs as discrete grains, associated with quartz and albite in apparent equilibrium (Fig. 6g,h). Some grains have jadeite-poor outer zones. Hematite flakes are aligned parallel to the foliation. Calcite locally forms rod-shaped crystals

indicative of the derivation from aragonite (e.g. Brady *et al.*, 2004; Topuz *et al.*, 2006).

Metacherts are thinly layered and consist of quartz + phengite \pm lawsonite \pm albite \pm piemontite + chlorite + titanite + hematite. Marbles are white to pink and, apart from calcite, contain quartz, albite, phengite and Fe-hydroxides.

Serpentinities are made of serpentine + magnetite + chlorite + minor clinopyroxene, and are free of any relict igneous phases. The XRD studies on three serpentinite samples showed that antigorite is the only serpentine mineral.

Metaroddingites are fine-grained and massive, and consist of garnet + clinopyroxene \pm chlorite \pm apatite \pm serpentine \pm opaques.

MINERAL COMPOSITIONS

Mineral analyses were carried out on 20 samples with a CAMECA-SX51 electron microprobe equipped with five wavelength-dispersive spectrometers at the Mineralogical Institute of the University of Heidelberg. Well-characterized natural and synthetic oxide and silicate minerals were used for calibration before each measurement session. Standard operating conditions were 15 kV accelerating voltage, 20 nA beam current and 10 s counting time for all elements. However, counting times during titanite analyses were 20 s for Mg, Ca and Al and 30 s for Ti. A beam size of ~ 1 μm was normally used in all analyses. Larger grains of albite were analysed with a beam size of ~ 10 μm to minimize alkali loss due to volatilization, whereas finer grains were analysed with a small beam size. Raw data were corrected for matrix effects with the help of the PAP algorithm (Pouchou & Pichoir, 1984, 1985), implemented by CAMECA.

Sodic pyroxene (Na–Px) in the metadiabase samples is characterized by highly variable jadeite (Jd_{31-75}) and generally low aegirine contents (Ae_{00-06}) (Tables 1 & 2; Fig. 7a). In the blueschists, jadeite contents are generally lower (Jd_{07-67}) and aegirine contents are highly variable (Fig. 7b). Sodic pyroxene from the metadiabases mostly plots within the miscibility gaps along the augite–jadeite join (e.g. Carpenter, 1980; Tsujimori, 1997; Matsumoto & Hirajima, 2005; Tsujimori *et al.*, 2005; Green *et al.*, 2007). This may be the result of fine submicroscopic intergrowth of jadeite- and augite-rich Na-pyroxene.

Relict magmatic clinopyroxene is found in all metadiabase and in three blueschist samples (Table 1). Those in the blueschists are richer in Ti and Al than those in the metadiabase samples (Fig. 7c). The $\text{Mg}/(\text{Mg} + \text{Fe}^{2+})$ values of the relict magmatic clinopyroxenes range from 0.42 to 0.91 in the metadiabases and 0.50 to 0.84 in the blueschists. The intrasample variation of the $\text{Mg}/(\text{Mg} + \text{Fe}^{2+})$ values may be as high as 0.30. The lowest $\text{Mg}/(\text{Mg} + \text{Fe}^{2+})$ values are shown by the clinopyroxene overgrowths (Fig. 5a). In addition, the metadiabase samples contain igneous magnesiohornblende with relatively high Ti and Al contents.

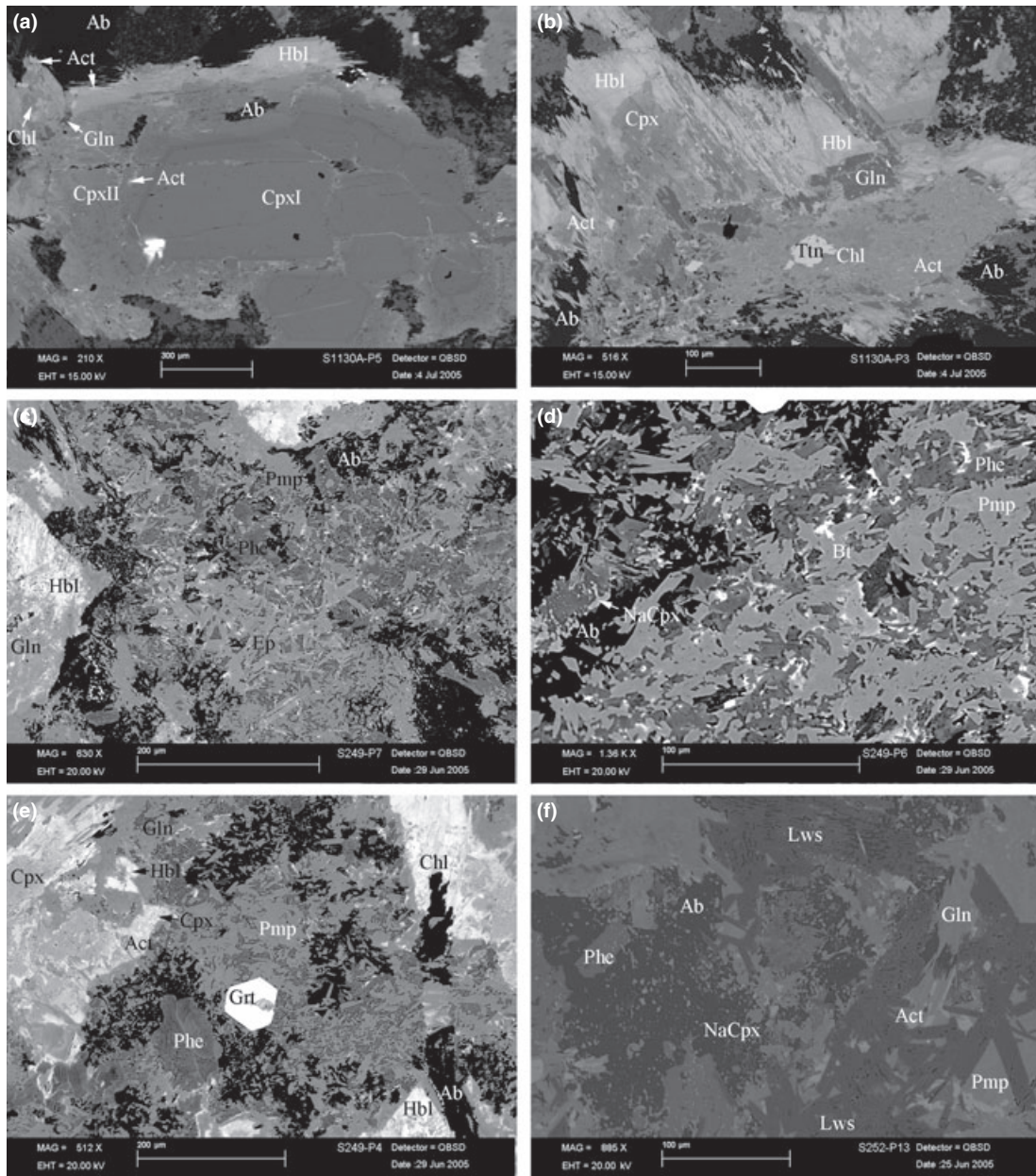


Fig. 5. Photomicrographs of metadiabase samples: (a) relict igneous clinopyroxene (CpxI) is overgrown by late-stage igneous clinopyroxene (CpxII) and hornblende (Hbl). Both Cpx and Hbl are irregularly replaced by actinolite (Act), chlorite (Chl) and albite (Ab); sample 1130A. (b) Relict igneous Cpx and Hbl, partially replaced by glaucophane (Gln), Act, Chl and titanite (Ttn); sample 1130A. (c) Patchy intergrowth of epidote (Ep), pumpellyite (Pmp), phengite (Phe) and albite (Ab) in a former plagioclase; sample 243. (d) Intergrowth of Pmp, Phe, Ab, sodic pyroxene (Na-Px) and tiny grains of biotite (Bt); sample 243. (e) Idioblastic garnet (Grt) within intergrowth of Pmp, Phe and Ab; sample 243. (f) Intergrowth of lawsonite (Lws), Na-Px, Phe, Act and Gln; sample 252.

Glaucophane–magnesioriebeckite has variable compositions (Table 3, Fig. 8), although in all samples the zonation of individual grains is similar: Cores are richer in $X_{\text{Fe}^{3+}}$ [$=\text{Fe}^{3+}/(\text{Fe}^{3+} + \text{Al}^{\text{VI}})$; Fe^{3+} is calculated as 2-Al^{VI}] than rims. In the blueschists, there is a wide range of $X_{\text{Fe}^{3+}}$ from 0.0 to ~ 0.9 , while in the metadiabase samples, $X_{\text{Fe}^{3+}}$ of glaucophane is mostly ≤ 0.30 . For most of the samples, $\text{Mg}\#$ [$=\text{Mg}/(\text{Mg} +$

$\text{Fe}^{2+})$] correlates weakly with $X_{\text{Fe}^{3+}}$. Furthermore, there is a positive correlation of $X_{\text{Ca}} = \text{Ca}/(\text{Na} + \text{Ca})$ with $X_{\text{Fe}^{3+}}$ for each sample. In the metadiabases, the regression lines go through the origin, while in the blueschists, the $X_{\text{Fe}^{3+}}$ intercepts may be very different from sample to sample.

Actinolite is only present in the four metadiabases and in three blueschists (Table 1). Larger

Table 1. Modal abundances of minerals and jadeite contents in Na-pyroxene in blueschist facies rocks from Sarköy area, Thrace, NW Turkey.

Sample	Cpx ^a	Hbl ^b	Na-Px	Jd (%)	Ab	Gln ^b	Lws	Phe	Act	Pmp	Ep	Chl	Qtz	Ttn	Grt	Bt	Ap	Cal	Hem	Pie	Di
<i>Carbonate-poor blueschists</i>																					
356A	10	–	13	07–38	4	31	28	4	–	–	–	–	4	5	–	–	1	–	–	–	–
356B	–	–	–	–	6	42	35	3	–	–	–	4	3	3	–	–	1	–	–	–	–
356C	–	–	–	–	6	40	30	7	–	–	–	–	11	7	–	–	1	–	–	–	–
356D	13	–	15	17–67	6	25	25	2	–	–	–	6	3	5	–	–	1	–	–	–	–
359	–	–	15	08–23	11	15	30	4	–	–	3	8	11	2	–	–	1	–	–	–	–
363	–	–	–	–	6	25	35	7	4	–	–	6	5	7	–	–	1	–	–	–	–
364	7	–	15	25–40	sec	16	25	3	11	–	–	14	3	3	–	–	1	–	–	–	–
1132A	–	–	–	–	8	25	30	10	–	–	3	7	10	10	–	–	1	3	–	–	–
1133A	–	–	–	–	6	20	25	20	–	–	3	12	10	20	–	–	1	–	–	–	–
<i>Carbonate-rich blueschists</i>																					
362	–	–	8	18–43	7	18	10	28	–	–	4	4	7	4	–	–	1	28	2	–	–
1132B	–	–	17	10–48	7	14	8	12	–	–	6	3	7	2	–	–	1	24	3	–	–
1133B	–	–	–	–	18	9	23	10	3	–	–	6	18	2	–	–	1	16	–	–	–
1287	–	–	25	27–69	11	7	15	13	–	–	2	2	11	2	–	–	1	18	–	–	–
<i>Metadiabases type I</i>																					
252	20	5	6	61–75	6	8	15	2	18	13	–	–	4	2	–	–	1	–	–	–	–
1275	25	10	–	–	4	9	19	3	23	4	–	1	1	1	–	–	1	–	–	–	–
<i>Metadiabases type II</i>																					
243	17	14	5	31–46	5	5	–	2	16	19	5	–	4	2	4	1	1	–	–	–	–
1130A	10	16	–	–	12	5	–	2	15	20	6	5	1	3	3	1	1	–	–	–	–
<i>Quartzite (Metachert)</i>																					
1131	–	–	–	–	10	–	–	30	–	–	–	5	43	–	–	–	–	–	7	5	–
<i>Metarodinite</i>																					
1272B	–	–	–	–	–	–	–	–	–	–	–	20	10	–	50	–	–	–	–	–	20

Pie, piemontite.

^aRelict magmatic phase of protolith.^bGln stands for all members of the glaucophane–magnesioriebeckite series.

individual grains show a rimward decrease in Si and in Na_B.

Pumpellyite in the metadiabase samples is relatively rich in Al, compositionally similar to the newly approved mineral species pumpellyite-(Al) (Hatert *et al.*, 2007; Table 4; Fig. 9a). Comparable pumpellyite compositions were also described from the pumpellyite–actinolite subfacies and from blueschist facies rocks (Maruyama & Liou, 1988; El-Shazly, 1994; Topuz & Altherr, 2004).

Lawsonite in the blueschist samples shows a wide range of Fe₂O₃ contents (0.21–3.31 wt%; Table 4), while those from the metadiabase samples are relatively low in Fe₂O₃ (0.08–0.54 wt%). Overall, there is a correlation between Fe₂O₃ in lawsonite and X_{Fe³⁺} in glaucophane–magnesioriebeckite. Clinzoisite/epidote in metadiabase II has X_{Fe³⁺} [= Fe³⁺/(Al + Fe³⁺)] values of 0.01–0.02 (sample 243) and of 0.23–0.25 (1130A). In the blueschists, epidote is more Fe-rich (0.30–0.35) and some grains have elevated REE contents (up to 8 wt%).

Phengite in both blueschists and metadiabase samples is characterized by Si contents of 3.40–3.70 cations per formula unit (cpfu) (Table 5). Chlorite displays a narrow range of Mg/(Mg + Fe²⁺) ratios of 0.42–0.52 in the metadiabases, and of 0.48–0.72 in the blueschists (Table 5). Biotite in the metadiabase II samples is characterized by Mg/(Mg + Fe²⁺) values of 0.43–0.54 and extremely low Ti contents (<0.017 cpfu), suggesting a metamorphic origin (Table 5).

Titanite displays variable Fe₂O₃ and Al₂O₃ contents of 0.37–2.40 and 0.23–3.04 wt% respectively, in the

blueschists, and of 0.32–1.67 and 0.84–2.51 wt% respectively, in the metadiabases. The higher the X_{Fe³⁺} values of glaucophane–magnesioriebeckite, the higher the Fe₂O₃ content of titanite (not shown). Hematite from the blueschists has variable TiO₂ contents (2.26–2.35 wt%), similar to those described from lawsonite-bearing blueschists from the Tavşanlı zone, NW Turkey (Okay, 1980).

Garnet is present in metadiabase-II samples (Table 1). It is characterized by the compositional range Alm_{34–52}Pyp_{00–02}Sps_{00–15}Grs_{33–66} (Fig. 9b) and has small amounts of TiO₂ (≤0.57 wt%; Table 6). Within some garnet grains, a core (Alm_{34–40}Pyp_{00–01}Sps_{00–01}Grs_{58–66}) is visible, separated from an overgrowth (Alm_{47–52}Pyp_{01–02}Sps_{08–15}Grs_{33–44}) by a sharp boundary. In these samples, garnet is in coexistence with pumpellyite, an assemblage that is also described by Okay (1982) and Zhang *et al.* (2001). However, garnet in the latter occurrences is a member of the andradite–grossularite series.

METAMORPHIC CONDITIONS

Quantification of *P–T* conditions of very low-grade metamorphism is difficult, primarily due to a lack of reliable thermodynamic data and mixing models for equilibria involving minerals such as glaucophane, pumpellyite and chlorite as well as slow reaction kinetics (e.g. Liou *et al.*, 1985, 1987; Evans, 1990; Frey *et al.*, 1991; Schiffman & Day, 1999). Therefore, *P–T* estimates on such rocks are only an approximation. Here, the conditions are constrained by comparing the mineral

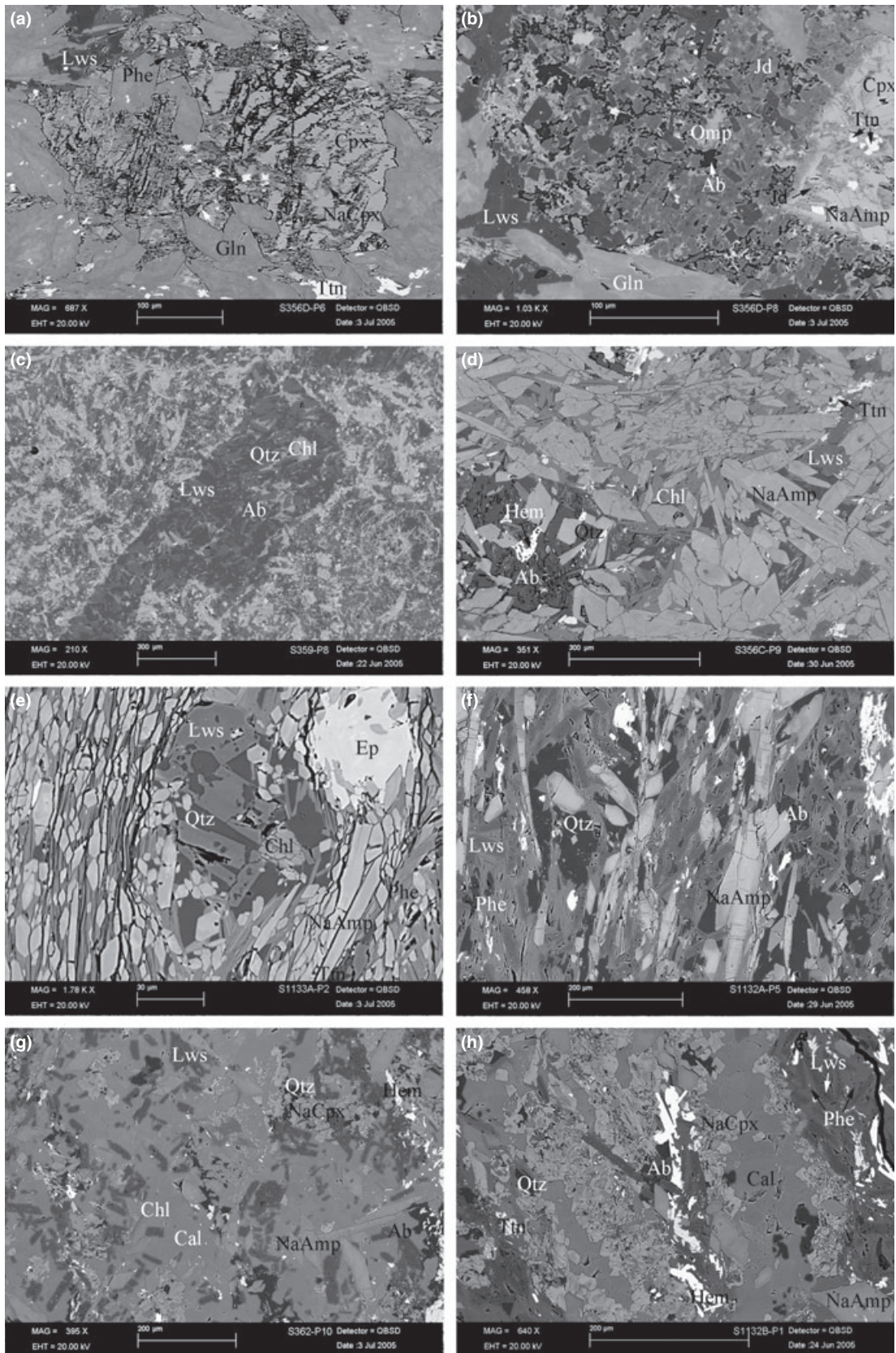


Table 2. Selected analyses of sodic pyroxene in blueschist facies rocks from Sarköy area, Thrace, NW Turkey.

Sample	356A	356A	356D	356D	359	364	364	362	362	1132B	1132B	1287	1287	252	252	243
Analyses	76	81	22	92	69	37	119	69	60	49	51	4	39	31	32	12
SiO ₂	53.78	54.53	54.38	57.30	53.65	53.70	55.89	53.69	55.02	53.36	55.46	54.33	57.60	56.36	57.26	55.42
TiO ₂	0.04	0.41	0.11	–	0.41	0.25	0.12	0.27	0.64	–	0.37	0.06	0.01	0.01	–	0.05
Al ₂ O ₃	1.64	8.77	3.85	16.06	5.30	5.66	9.44	4.08	9.88	2.18	11.12	6.12	16.29	14.51	16.96	10.83
Cr ₂ O ₃	–	–	0.01	–	0.12	0.06	0.14	0.31	0.01	0.03	0.02	–	–	–	0.05	0.04
Fe ₂ O ₃	8.75	17.48	5.19	7.29	20.52	4.94	3.58	21.91	16.41	19.04	14.03	22.45	11.32	1.39	–	–
FeO	5.18	3.57	7.78	3.65	0.42	4.51	5.53	2.03	1.89	3.69	3.67	0.32	0.18	5.12	5.68	7.73
MnO	0.43	–	0.64	0.04	0.14	0.35	0.21	0.06	–	0.01	0.03	–	0.01	0.24	0.27	0.13
MgO	9.15	0.50	8.52	0.72	3.69	9.69	6.94	2.36	1.13	4.57	0.71	1.70	0.40	3.53	2.45	5.50
CaO	17.02	0.77	15.43	1.62	5.98	14.68	10.23	3.72	1.98	7.75	2.03	2.70	0.68	9.44	7.10	13.17
Na ₂ O	4.45	12.93	4.68	13.24	10.72	5.04	7.69	11.51	12.93	9.07	12.73	12.51	14.46	9.37	10.49	6.74
K ₂ O	–	0.06	0.01	0.02	–	0.04	0.03	–	–	–	0.01	0.07	0.01	0.07	0.06	–
Total	100.42	98.99	100.61	99.95	100.95	98.89	99.79	99.94	99.89	99.67	100.18	100.25	100.97	100.05	100.31	99.61

Cations on the basis of 6 oxygen ions and 4 cations

Si	2.00	2.02	2.01	2.02	1.97	1.98	2.01	2.01	2.00	2.01	2.01	2.00	2.01	2.00	2.01	2.01
Ti	0.00	0.01	0.00	0.00	0.01	0.01	0.00	0.01	0.02	0.00	0.01	0.00	0.00	0.00	0.00	0.00
Al	0.07	0.38	0.17	0.67	0.23	0.25	0.40	0.18	0.42	0.10	0.47	0.27	0.67	0.61	0.70	0.46
Cr	0.00	0.00	0.00	0.00	0.00	0.00	0.00	0.01	0.00	0.00	0.00	0.00	0.00	0.00	0.00	0.00
Fe ³⁺	0.25	0.49	0.14	0.19	0.57	0.14	0.10	0.62	0.45	0.54	0.38	0.62	0.30	0.04	0.00	0.00
Fe ²⁺	0.16	0.11	0.24	0.11	0.01	0.14	0.17	0.06	0.06	0.12	0.11	0.01	0.01	0.15	0.17	0.23
Mn	0.01	0.00	0.02	0.00	0.00	0.01	0.01	0.00	0.00	0.00	0.00	0.00	0.00	0.01	0.01	0.00
Mg	0.51	0.03	0.47	0.04	0.20	0.53	0.37	0.13	0.06	0.26	0.04	0.09	0.02	0.19	0.13	0.30
Ca	0.68	0.03	0.61	0.06	0.24	0.58	0.40	0.15	0.08	0.31	0.08	0.11	0.03	0.36	0.27	0.51
Na	0.32	0.93	0.34	0.91	0.76	0.36	0.54	0.83	0.91	0.66	0.89	0.89	0.98	0.65	0.71	0.47
K	0.00	0.00	0.00	0.00	0.00	0.00	0.00	0.00	0.00	0.00	0.00	0.00	0.00	0.00	0.00	0.00

assemblages with those in the system NCMASH, whereby the petrogenetic grids calculated by Schiffman & Day (1999) and Bucher & Frey (2002) are used.

Helvatepe blueschists

In all blueschist samples, glaucophane coexists with lawsonite. The stability field of this sub-paragenesis is on the high-*P*/low-*T* side of the reactions (Fig. 10):



and



In the NCMASH system, these two reactions restrict the *P*–*T* conditions of metamorphism to pressures of ≥ 0.67 GPa at 200 °C and ≥ 0.78 GPa at 300 °C (Fig. 10). With the introduction of Fe²⁺ and Fe³⁺, however, reactions (1) and (2) will be displaced to lower pressures, thereby enlarging the *P*–*T* field for glaucophane–lawsonite-bearing assemblages (Liou *et al.*, 1985, 1987; Maruyama *et al.*, 1986).

Bucher & Frey (2002) suggest the reaction



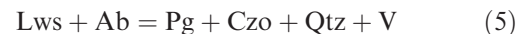
which is located at ~ 0.4 GPa/200 °C and terminates at ~ 0.85 GPa/300 °C (fig. 9.9 in Bucher & Frey, 2002). In one of the investigated samples (363), the paragenesis glaucophane + lawsonite + actinolite + albite + chlorite was observed, indicating that metamorphic conditions were near to those of reaction (3).

Since albite + chlorite + quartz forms a common sub-paragenesis in most of the investigated blueschists (Table 1) and paragonite is absent, the reaction



was not crossed to the high-pressure side, thus restricting metamorphic conditions to < 0.7 GPa at 200 °C and 0.85 GPa at 300 °C (Bucher & Frey, 2002; not shown in Fig. 10).

Likewise, the rocks contain Lws + Ab, and therefore the reaction



was not crossed. This reaction is fairly steep in the *P*–*T* field, i.e. at 0.3 GPa/250 °C and 0.8 GPa/320 °C (Fig. 10).

Seven blueschist samples contain sodic pyroxene, and in six of these samples, it occurs with albite and

Fig. 6. Photomicrographs of blueschist samples: (a) relict Cpx is replaced by Na–Px (locally together with Phe and Gln) along cracks; sample 356D. (b) Igneous Cpx is replaced by glaucophane–magnesianriebeckite (NaAmp) and Ttn (left margin) and overgrown by jadeitic pyroxene (Jd) and Lws. This jadeite-rich pyroxene is locally replaced by omphacite (Omp) and Ab; sample 356D. (c) Former plagioclase phenocryst is pseudomorphically replaced by mixture of Lws, quartz (Qtz), Ab and Chl; sample 359. (d) Metamorphic intergrowth of glaucophane–magnesianriebeckite (NaAmp), Chl, Lws, Ab, Qtz and hematite (Hem); sample 356C. (e) Epidote (Ep) with inclusions of NaAmp, coexisting with Lws + Qtz + Chl; sample 1133A. (f) Paragenesis of NaAmp + Lws + Phe + Qtz + Ab. Crystals of NaAmp are zoned with cores being richer in Fe³⁺ and Ca than the rims; sample 1132A. (g) Calcite-rich blueschist with calcite (Cal), NaAmp, Lws, Qtz, Chl, Hem; sample 362. (h) Na–Px coexisting with Ab + Lws + Cal + Gln + Hem ± Qtz; sample 1132B. Note that Phe is intergrown with Lws (right margin).

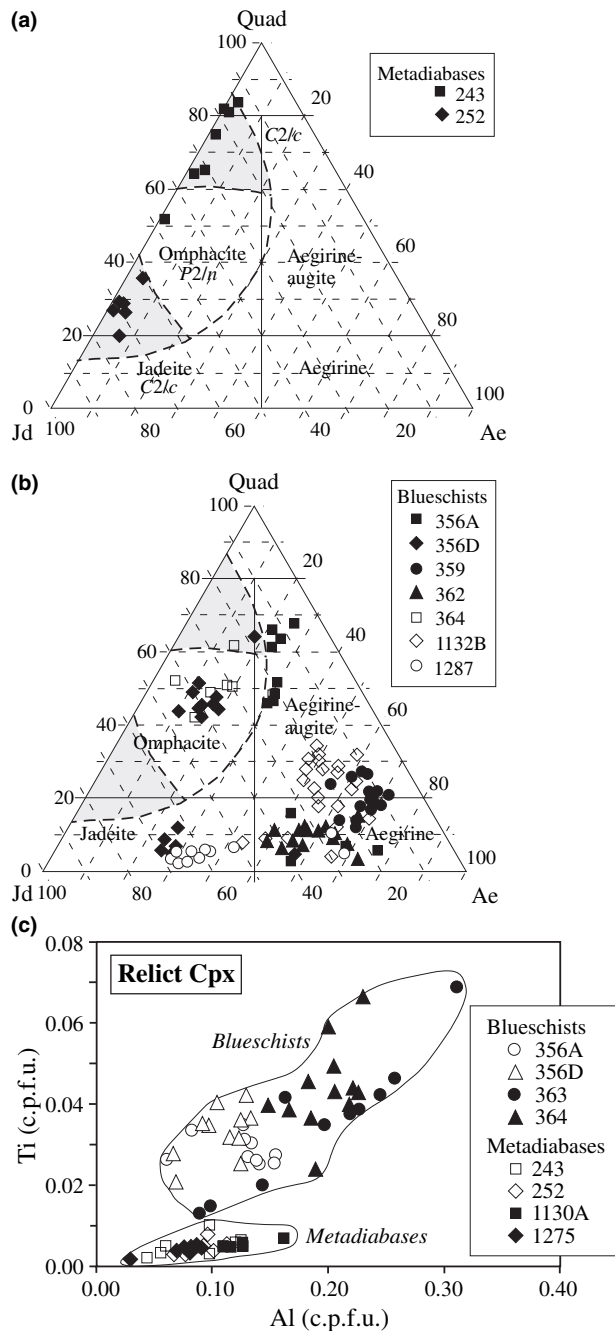


Fig. 7. Compositional variation of sodic pyroxene from metadiabases (a) and blueschists (b) plotted in Quad–Jd–Ae ternary diagram. End-member components are calculated according to Marimoto *et al.* (1988). Thick dashed lines represent the phase relations in the Quad–Jd–Ae system according to Carpenter (1980), and the grey fields are the miscibility gaps. (c) Ti *v.* Al in cations per formula unit (c.p.f.u.) for igneous clinopyroxene from blueschist and metadiabase samples.

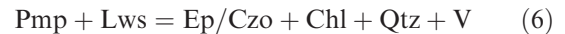
quartz (Table 1). Jadeite contents in the pyroxene of these samples display relatively large variations, possibly due to the fact that not all Na-pyroxene grains coexist with albite and quartz. Furthermore,

low-jadeite pyroxene often surrounds high-jadeite pyroxene indicating its secondary nature. Maximum jadeite contents of Na-Px in these samples were found to range from 23 to 69 mol.% (Table 1). These values restrict metamorphic pressures to $< \sim 0.6$ GPa at 200 °C and ~ 0.85 GPa at 300 °C (e.g. Holland, 1983).

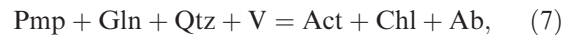
Summarizing the information from the different reactions, we conclude that the blueschists were metamorphosed at ~ 0.7 – 0.85 GPa and 270–310 °C. These *P*–*T* conditions are within the stability field of aragonite. This is supported by the occurrence of rod-shaped calcite pseudomorphs after former aragonite (e.g. samples 1132B and 1133B).

Sarikaya metadiabases (type I)

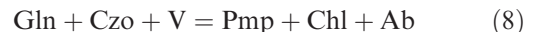
The coexistence of pumpellyite + lawsonite and the absence of epidote in these rocks indicates that the reaction



was not crossed (Fig. 10). Reaction (6) is supposed to lie at slightly lower temperatures than reaction (5), i.e. at ~ 290 °C (Schiffman & Day, 1999; fig. 9.6 in Bucher & Frey, 2002). The introduction of Fe will shift this reaction to somewhat lower temperatures. Furthermore, the parageneses of these metadiabase samples (Table 1) suggest temperatures that were those of the reaction



which, in the system NCMASH, is located at ~ 0.53 GPa/200 °C and 0.78 GPa/380 °C (Schiffman & Day, 1999). Reactions (6) and (7) cross each other at ~ 0.65 GPa/290 °C (Fig. 10). The maximum pressure stability limit of pumpellyite is given by reaction (1) at low temperatures and by the reaction



at temperatures above reaction (6). Reaction (8) is a flat reaction in *P*–*T* space and is located at ~ 0.8 GPa/300 °C (Fig. 10). In addition, the coexistence of Na-pyroxene (Jd_{61–75}) with albite suggests pressures below ~ 0.8 GPa. Quartz in these rocks (Table 1) was not found in coexistence with Na-pyroxene.

Antigorite is stable at temperatures above 200–250 °C at the expense of chrysotile and lizardite (e.g. O'Hanley, 1996, pp. 33 and 160). Its occurrence in the Sarikaya serpentinite along with type-I metadiabase is compatible with the view that both the serpentinite and the metadiabase were subjected to the blueschist facies conditions.

In conclusion, the peak metamorphic conditions of the Sarikaya serpentinite body and associated metadiabases are estimated to 0.65–0.75 GPa and ≤ 290 °C.

Table 3. Selected chemical analyses of glaucophane–magnesioriebeckite in blueschist facies rocks from Sarköy area, Thrace, NW Turkey.

Sample	356A	356A	356B	356D	356D	363	363	1132A	1132A	1132B	1132B	1133A	1133A	243	252	1275
Analyses	77	9	42	14	18	2	6	11	16	132	123	59	14	84	24	56
Area	Rim	Core	Core	Rim	Core	Rim	Core	Rim	Core	Rim	Core	Rim	Core	Rim	Rim	Rim
SiO ₂	56.94	56.14	55.39	56.74	55.29	56.88	55.87	57.19	55.54	56.52	56.32	56.61	55.57	56.55	55.82	56.63
TiO ₂	0.06	0.11	0.10	0.12	0.10	0.27	0.11	–	0.10	0.03	–	–	–	0.01	–	0.02
Al ₂ O ₃	8.37	4.89	4.39	9.36	5.31	10.01	5.67	6.43	2.72	4.99	1.22	5.73	1.58	11.72	11.85	11.87
Cr ₂ O ₃	0.04	0.01	0.02	0.01	0.01	–	0.02	0.06	0.02	–	–	–	–	0.00	0.02	0.00
Fe ₂ O ₃	4.67	6.80	11.55	2.90	4.91	1.97	4.52	8.53	12.42	10.12	9.89	8.43	9.32	0.72	1.92	4.13
FeO	11.37	11.01	10.69	13.78	14.07	13.29	11.05	7.56	10.03	7.55	9.07	9.79	11.16	12.74	13.38	10.23
MnO	0.22	0.39	0.22	0.40	0.46	0.15	0.31	0.15	0.14	0.57	0.17	0.11	0.20	0.03	0.09	0.17
MgO	8.19	9.67	7.78	7.26	8.79	7.39	9.84	10.09	9.40	10.45	12.91	9.22	11.27	7.55	6.00	7.93
CaO	0.36	2.27	0.86	0.60	3.42	0.71	5.03	0.28	0.96	0.96	5.19	0.49	3.73	1.41	0.88	0.81
Na ₂ O	7.12	5.90	6.94	6.82	5.05	6.95	5.01	7.29	6.49	6.72	4.32	6.98	4.76	6.70	7.12	6.99
K ₂ O	0.01	0.02	0.02	0.03	0.05	0.03	0.03	0.02	0.03	–	0.04	0.03	0.10	0.02	0.04	0.00
H ₂ O	2.13	2.10	2.09	2.13	2.08	2.14	2.11	2.14	2.08	2.13	2.12	2.11	2.08	2.15	2.12	2.15
Total	99.45	99.29	100.03	100.13	99.54	99.79	99.56	99.74	99.93	100.04	101.26	99.50	99.77	99.62	99.25	99.52

Cations on the basis of a total of 15 cations (excluding K), 23 oxygen ions and 2 OH

Si	8.02	8.03	7.96	7.98	7.97	7.98	7.96	8.00	7.99	7.96	7.96	8.03	8.02	7.90	7.88	7.75
Ti	0.01	0.01	0.01	0.01	0.01	0.03	0.01	0.00	0.01	0.00	0.00	0.00	0.00	0.00	0.00	0.00
Al	1.39	0.82	0.74	1.55	0.90	1.66	0.95	1.06	0.46	0.83	0.20	0.96	0.27	1.93	1.97	1.95
Cr	0.00	0.00	0.00	0.00	0.00	0.00	0.00	0.01	0.00	0.00	0.00	0.00	0.00	0.00	0.00	0.00
Fe ³⁺	0.49	0.73	1.25	0.31	0.53	0.21	0.48	0.90	1.34	1.07	1.05	0.90	1.01	0.08	0.20	0.43
Fe ²⁺	1.34	1.32	1.28	1.62	1.70	1.56	1.32	0.88	1.21	0.89	1.07	1.16	1.35	1.49	1.58	1.19
Mn	0.03	0.05	0.03	0.05	0.06	0.02	0.04	0.02	0.02	0.07	0.02	0.01	0.02	0.00	0.01	0.02
Mg	1.72	2.06	1.66	1.52	1.89	1.55	2.09	2.11	2.02	2.19	2.72	1.95	2.42	1.57	1.26	1.65
Ca	0.05	0.35	0.13	0.09	0.53	0.11	0.77	0.04	0.15	0.15	0.79	0.07	0.58	0.21	0.13	0.12
Na	1.94	1.64	1.93	1.86	1.41	1.89	1.38	1.98	1.81	1.83	1.18	1.92	1.33	1.82	1.95	1.89
K	0.00	0.00	0.00	0.00	0.01	0.00	0.01	0.00	0.01	0.00	0.01	0.01	0.02	0.00	0.01	0.00

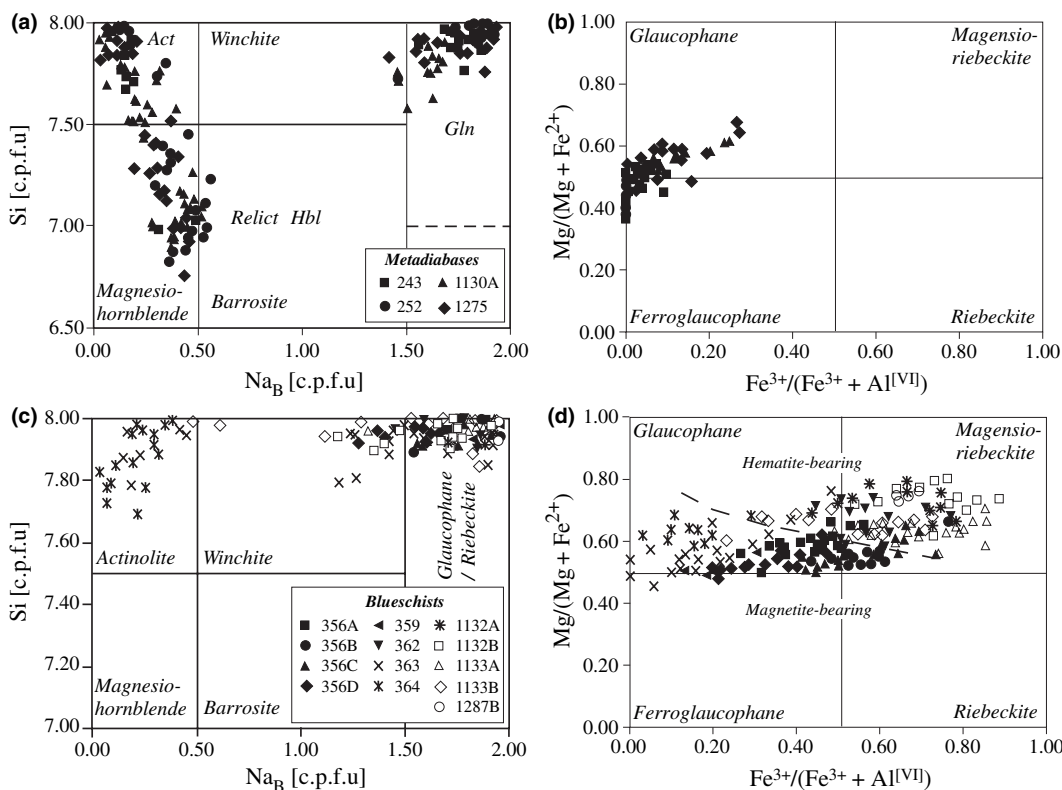


Fig. 8. Compositional variation of amphibole from the metadiabases and blueschists, plotted in Na_B v. Si (a and c) and Fe³⁺/(Fe³⁺ + Al^{VI}) v. Mg/(Fe²⁺ + Mg) (b and d). Fe³⁺ contents and site assignments of amphibole were calculated, assuming Σ(Si + Ti + Al + Cr + Fe²⁺ + Fe³⁺ + Mn + Mg) = 13.00 pro 23 oxygen. The dividing lines were adopted from Leake *et al.* (1997).

Table 4. Selected analyses of pumpellyite, lawsonite and epidote in blueschist facies rocks from Sarköy area, Thrace, NW Turkey.

Mineral	Pmp	Pmp	Pmp	Pmp	Pmp	Pmp	Lws	Lws	Lws	Lws	Lws	Lws	Ep	Ep	Ep	Ep
Sample	252	252	1275	243	243	1130A	252	356A	359	1132A	1132B	1275	359	1132B	243	1130A
Analyses	51	57	46	113	172	77	10	69	1	30	50	90	4	150	3	32
SiO ₂	37.44	38.35	37.88	37.49	37.58	37.12	39.15	39.46	38.95	39.55	39.19	39.80	36.70	37.02	39.55	37.53
TiO ₂	0.03	0.01	–	0.12	0.03	0.06	0.14	0.07	0.29	0.16	0.02	0.09	0.26	0.08	–	0.09
Al ₂ O ₃	26.85	26.22	25.37	25.87	25.63	26.97	31.85	30.82	28.93	30.12	29.22	31.39	18.58	20.73	32.47	23.76
Cr ₂ O ₃	–	–	0.04	0.05	–	–	0.01	–	0.03	0.02	0.02	0.01	–	0.04	–	–
Fe ₂ O ₃	–	–	–	–	–	–	0.14	1.46	2.59	2.81	3.56	0.20	18.78	16.94	1.08	12.24
FeO	2.74	5.13	3.40	3.65	3.75	3.34	–	–	–	–	–	–	–	–	–	–
MnO	0.20	0.24	0.19	0.19	0.21	0.33	–	–	–	–	0.02	0.03	0.04	0.10	0.03	0.04
MgO	1.70	0.64	2.66	2.04	2.36	1.88	–	–	–	–	–	0.06	–	–	0.06	0.08
CaO	22.57	21.78	22.42	22.57	22.35	22.17	17.58	17.03	16.82	17.30	16.57	16.41	22.66	22.70	23.46	23.34
Na ₂ O	0.07	0.20	0.11	0.16	0.27	0.14	–	–	–	–	0.05	0.02	0.03	0.03	0.01	0.04
K ₂ O	–	–	0.02	0.01	–	–	0.01	0.01	–	0.02	–	0.15	–	–	0.03	–
H ₂ O	7.58	7.60	7.58	7.57	7.57	7.58	11.53	11.50	11.28	11.57	11.39	11.48	1.82	1.85	1.95	1.87
Total	99.18	100.17	99.67	99.74	99.75	99.59	100.42	100.34	98.89	101.55	100.03	99.65	98.85	99.49	98.65	98.98

Cations (basis see below)

Si	2.96	3.03	3.00	2.97	2.97	2.94	2.04	2.06	2.08	2.05	2.06	2.08	3.01	3.00	3.03	3.00
Ti	0.00	0.00	0.00	0.01	0.00	0.00	0.01	0.00	0.01	0.01	0.00	0.00	0.02	0.00	0.00	0.01
Al	2.50	2.44	2.36	2.41	2.39	2.51	1.95	1.90	1.82	1.84	1.81	1.93	1.80	1.98	2.93	2.24
Cr	0.00	0.00	0.00	0.00	0.00	0.00	0.00	0.00	0.00	0.00	0.00	0.00	0.00	0.00	0.00	0.00
Fe ³⁺	0.00	0.00	0.00	0.00	0.00	0.00	0.01	0.06	0.10	0.11	0.14	0.01	1.16	1.03	0.06	0.74
Fe ²⁺	0.18	0.34	0.22	0.24	0.25	0.22	0.00	0.00	0.00	0.00	0.00	0.00	0.00	0.00	0.00	0.00
Mn	0.01	0.02	0.01	0.01	0.01	0.02	0.00	0.00	0.00	0.00	0.00	0.00	0.00	0.01	0.00	0.00
Mg	0.20	0.08	0.31	0.24	0.28	0.22	0.00	0.00	0.00	0.00	0.00	0.00	0.00	0.00	0.01	0.01
Ca	1.91	1.84	1.90	1.91	1.90	1.88	0.98	0.95	0.96	0.96	0.93	0.92	1.99	1.97	1.93	2.00
Na	0.01	0.03	0.02	0.02	0.04	0.02	0.00	0.00	0.00	0.00	0.00	0.00	0.00	0.00	0.00	0.01
K	0.00	0.00	0.00	0.00	0.00	0.00	0.00	0.00	0.00	0.00	0.00	0.01	0.00	0.00	0.00	0.00

Formulae were calculated on the basis of: 12 oxygen, 2 OH and 1 H₂O for Pmp; 8 oxygen, 1 H₂O and 2 OH for Lws; and 12.5 oxygen and 1 OH for Ep; total Fe is assumed to be ferrous in Pmp and ferric in Lws and Ep.

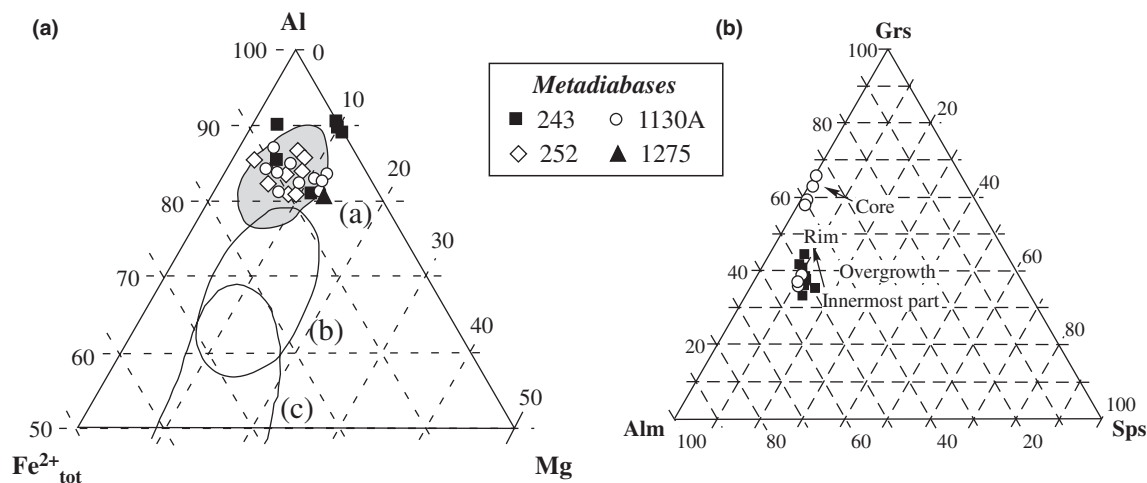


Fig. 9. (a) Pumpellyite compositions from metadiabase samples plotted in a Fe_{tot}–Al–Mg ternary diagram. Fields (1) through (3) stand for pumpellyite compositions from (1) Taveyannaz Formation (pumpellyite–actinolite facies) and Saih Hatat, Oman (blueschist facies metabasalts), (2) Olympic Peninsula, USA (prehnite–pumpellyite facies) and (3) East Taiwan ophiolite (zeolite facies). (b) Compositional variation of garnet in the Grs–Alm–Sps triangle.

Metadiabase olistolith (type II)

In these samples, pumpellyite is accompanied by epidote, and lawsonite is absent. This suggests *P*-dependent temperatures that (i) have exceeded those of reaction (6) and (ii) were near to those of reaction (7). This suggests slightly higher temperatures, compared with those of metadiabases I (Fig. 10).

GEOCHRONOLOGY

To date the timing of the high-*P/T* metamorphism, incremental ⁴⁰Ar/³⁹Ar dating on phengite-rich aliquots and Rb–Sr dating on phengite–whole rock were carried out on two samples devoid of any relict texture. Sample 1131 is a fine-grained metachert comprising quartz, phengite, chlorite, piemontite, albite and

Table 5. Selected analyses of chlorite, phengite and biotite in blueschist facies rocks from Sarköy area, Thrace, NW Turkey.

Mineral	Chl	Chl	Chl	Chl	Chl	Phe	Bt									
Sample	356B	359	363	364	1133A	356A	356B	356D	359	363	364	1132A	1132B	1275	1130A	1130A
Analyses	38	3	20	27	37	55	58	43	46	50	68	65	39	64	76	127
SiO ₂	27.55	28.29	27.01	29.10	28.03	53.43	53.46	54.03	55.47	52.94	56.16	52.99	52.14	55.23	51.32	38.18
TiO ₂	–	0.07	0.01	0.07	0.04	0.05	0.18	0.27	0.02	0.06	0.06	0.09	0.09	0.07	0.04	0.09
Al ₂ O ₃	18.90	17.20	17.95	17.86	18.24	23.83	22.82	23.63	21.68	23.18	22.59	22.48	21.88	23.04	28.36	16.53
Cr ₂ O ₃	–	0.02	0.03	0.07	0.03	0.01	0.01	–	0.03	0.24	–	–	–	–	0.05	–
Fe ₂ O ₃	–	–	–	–	–	–	–	–	–	–	–	–	–	–	–	–
FeO	24.10	22.19	25.23	19.07	20.76	4.49	4.75	3.93	3.76	4.14	1.98	4.59	6.66	3.13	2.48	21.25
MnO	0.60	0.73	0.65	0.36	0.26	0.05	0.09	0.05	0.05	0.06	0.01	0.13	0.08	0.02	–	0.12
MgO	16.07	18.00	16.25	20.50	19.22	3.84	3.77	3.74	4.87	4.39	5.09	4.77	4.38	4.37	3.16	10.20
CaO	0.12	0.11	0.10	0.15	0.06	0.05	0.05	0.57	0.10	0.50	0.10	0.08	0.42	0.11	0.02	0.16
Na ₂ O	0.10	0.04	0.02	0.04	0.00	0.06	0.10	0.11	0.04	0.07	0.05	0.08	0.36	0.10	0.31	0.04
K ₂ O	0.13	0.03	0.04	0.01	0.01	10.36	10.54	10.09	10.19	10.33	10.22	10.31	9.87	10.15	10.31	8.70
H ₂ O	11.43	11.42	11.29	11.73	11.54	4.51	4.47	4.53	4.54	4.48	4.59	4.46	4.43	4.56	4.54	3.94
Total	99.00	98.09	98.60	98.96	99.75	100.69	100.25	100.94	100.75	100.37	100.85	100.08	100.30	100.78	100.58	99.22
<i>Cations (basis see below)</i>																
Si	2.89	2.97	2.87	2.97	2.91	3.55	3.58	3.57	3.67	3.54	3.67	3.56	3.53	3.63	3.39	2.90
Ti	0.00	0.01	0.007	0.01	0.00	0.00	0.01	0.01	0.00	0.00	0.00	0.00	0.00	0.00	0.00	0.01
Al	2.34	2.13	2.25	2.15	2.23	1.87	1.80	1.84	1.69	1.83	1.74	1.78	1.75	1.79	2.21	1.48
Cr	0.00	0.00	0.00	0.01	0.00	0.00	0.00	0.00	0.00	0.01	0.00	0.01	0.00	0.00	0.00	0.00
Fe ³⁺	0.00	0.00	0.00	0.00	0.00	0.00	0.00	0.00	0.00	0.00	0.00	0.00	0.00	0.00	0.00	0.00
Fe ²⁺	2.11	1.95	2.24	1.63	1.80	0.25	0.27	0.22	0.21	0.23	0.11	0.26	0.38	0.17	0.14	1.35
Mn	0.05	0.07	0.06	0.03	0.02	0.00	0.01	0.00	0.00	0.00	0.00	0.01	0.00	0.00	0.00	0.01
Mg	2.51	2.82	2.57	3.12	2.98	0.38	0.38	0.37	0.48	0.44	0.50	0.48	0.44	0.43	0.31	1.16
Ca	0.01	0.01	0.01	0.02	0.01	0.00	0.00	0.04	0.01	0.04	0.01	0.01	0.03	0.01	0.00	0.01
Na	0.02	0.01	0.00	0.01	0.00	0.01	0.01	0.01	0.01	0.01	0.01	0.01	0.05	0.01	0.04	0.01
K	0.02	0.00	0.01	0.00	0.00	0.88	0.90	0.85	0.86	0.88	0.85	0.88	0.85	0.85	0.87	0.84

Formulae were calculated on the basis of: 14 oxygen and 8 OH for Chl; 11 oxygen and 2 OH for Phe and Bt.

Table 6. Selected analyses of garnet in blueschist facies rocks from Şarköy area, Thrace, NW Turkey.

Mineral	Grt	Grt	Grt	Grt	Grt	Grt	Grt
Sample	243	243	243	1130A	1130A	1130A	1272B
Analyses	1	2	13	4	3	131	1
SiO ₂	37.84	38.13	37.48	37.06	38.20	37.15	38.01
TiO ₂	0.21	0.23	0.08	0.20	0.57	0.15	0.09
Al ₂ O ₃	21.01	20.97	20.95	21.07	20.07	21.06	17.93
Cr ₂ O ₃	0.03	0.01	–	0.02	0.01	–	–
Fe ₂ O ₃	–	–	–	–	–	–	7.19
FeO	21.25	22.30	23.36	23.07	16.25	23.30	–
MnO	3.60	6.65	5.72	4.88	0.17	4.54	0.34
MgO	0.33	0.33	0.43	0.47	0.00	0.48	1.04
CaO	15.70	12.52	11.52	12.84	24.69	12.93	34.70
Na ₂ O	0.02	0.01	0.03	–	–	–	–
K ₂ O	0.01	0.00	0.03	0.01	–	–	–
Total	100.01	101.13	99.59	99.61	99.96	99.61	99.29
<i>Cations based on 12 oxygen</i>							
Si	3.00	3.01	3.01	2.97	3.00	2.98	2.94
Ti	0.01	0.01	0.01	0.01	0.03	0.01	0.01
Al	1.96	1.95	1.98	1.99	1.86	1.99	1.64
Cr	0.00	0.00	0.00	0.00	0.00	0.00	0.00
Fe ³⁺	0.00	0.00	0.00	0.00	0.00	0.00	0.42
Fe ²⁺	1.41	1.47	1.57	1.55	1.07	1.56	0.00
Mn	0.24	0.44	0.39	0.33	0.01	0.31	0.02
Mg	0.04	0.04	0.05	0.06	0.00	0.06	0.12
Ca	1.33	1.06	0.99	1.10	2.08	1.11	2.88
Na	0.00	0.00	0.00	0.00	0.00	0.00	0.00
K	0.00	0.00	0.00	0.00	0.00	0.00	0.00
Total	8.01	8.00	8.00	8.02	8.04	8.02	8.02

apatite. From this sample, two different phengite concentrates were obtained (1131/1 & 1131/2). Sample 1132B is a fine-grained calcite-rich blueschist with glaucophane, lawsonite, Na-pyroxene, phengite,

chlorite, calcite, quartz, titanite and hematite. Phengite is intimately intergrown with lawsonite, Na-pyroxene and locally also glaucophane (Fig. 5h). Owing to fine-grain size of the samples and the matted nature of phengite, pure phengite separates could not be obtained. XRD studies revealed that the phengite separates from the two metachert samples contained considerable amounts of chlorite, piemontite and apatite, while that of the blueschist contained additional lawsonite and calcite.

Rb–Sr isotope analyses and incremental ⁴⁰Ar/³⁹Ar dating were performed with a Finnigan MAT-262 multicollector mass spectrometer at Tübingen and a MAT GD-150 gas mass spectrometer (0.38 T permanent magnet, 180°, 5 cm radius of curvature) at Heidelberg. Analytical techniques used in incremental ⁴⁰Ar/³⁹Ar and Rb–Sr dating are the same as outlined by Topuz *et al.* (2007) and Okay *et al.* (2006) respectively. ⁴⁰Ar/³⁹Ar age calculations were made against a new age of 328.5 ± 1.1 Ma for the used Bmsu/2 mineral standard (Schwarz & Trierloff, 2007). Analytical data are given in Tables 7 and 8 as well as Fig. 11 at 2σ error level.

The Rb–Sr two-point phengite–whole-rock isochron corresponds to age values of 85.9 ± 1.1 Ma (1131/2) and 86.5 ± 1.8 Ma (1132B). Incremental ⁴⁰Ar/³⁹Ar dating of the phengite samples 1131/1 and 1131/2 yield hump-shaped age spectra due to argon recoil between the different minerals (e.g. phengite and chlorite, see Topuz *et al.*, 2007), corresponding to integrated age values of 83.9 ± 1.4 (1.6) and

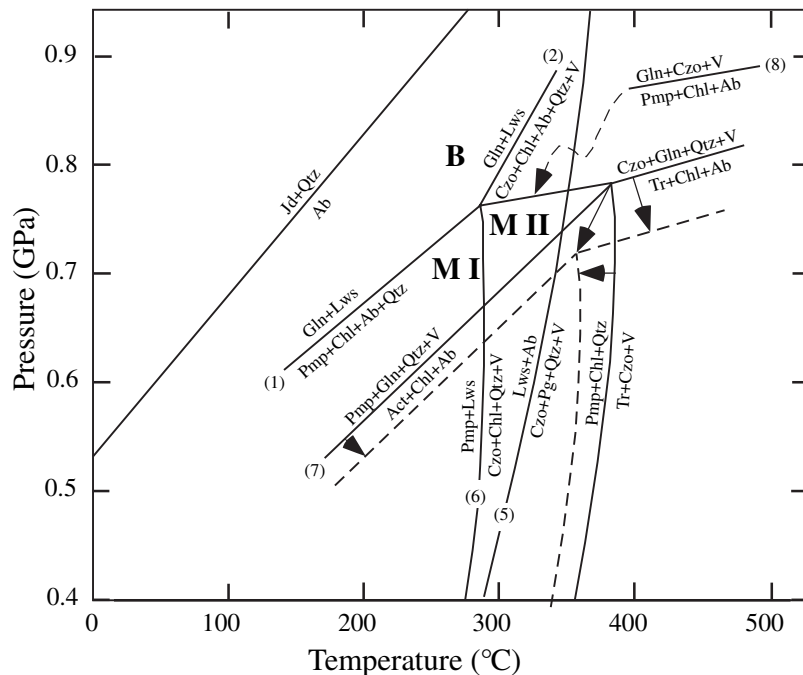


Fig. 10. P - T diagram (NCMASH) with reaction curves relevant for the investigated high- P / T metamorphic rocks from Schiffman & Day (1999) and Bucher & Frey (2002). Arrows mark the shift of certain equilibria with addition of Fe to the system. Metamorphic P - T conditions are marked by B (lawsonite-blueschists), M I (pumpellyite-lawsonite-bearing metadiabase) and M II (pumpellyite-epidote-bearing metadiabase).

85.2 ± 2.6 (2.7) Ma respectively (the first error is the uncertainty of the measurement; in parentheses, the monitor error is included). The K content of the phengite separates is 2.1 and 3.2 wt% respectively, calculated via the ^{39}Ar amount of the mineral standard and the sample. The elevated $^{37}\text{Ar}_{\text{Ca}}/^{39}\text{Ar}_{\text{K}}$ ratios and much larger uncertainty in the ages of the last incremental stage are caused by apatite and/or piemontite. Incremental $^{40}\text{Ar}/^{39}\text{Ar}$ dating on phengite-separate 1132B yielded a well-defined age spectrum, corresponding to an integrated age value of 85.3 ± 1.0 (1.2) Ma, indistinguishable from the total age of 1131 phengite samples (83.9 ± 1.4 and 85.2 ± 2.6 Ma). The plateau age calculated for the incremental steps 4–11 with more than 90% of ^{39}Ar released is 86.7 ± 1.1 (1.3) Ma. The K content of phengite 1132B is low (5.6 wt%), due to the presence of other Ca-bearing phases, but significantly higher than those of the 1131/1 and 1131/2 phengite samples. This is also reflected in the highly variable $^{37}\text{Ar}_{\text{Ca}}/^{39}\text{Ar}_{\text{K}}$ ratio of distinct incremental steps and the higher Sr concentration (Table 8). The impurity phases are nominally K-free, and their contribution to Ar budget is insignificant. All $^{40}\text{Ar}/^{39}\text{Ar}$ total ages are indistinguishable within the range of error. Samples 1131/1 and 1131/2, with low K contents, show hump-shaped spectra caused by high amounts of argon redistribution during irradiation. Sample 1132B with a higher K value has a flat spectrum indicating small amounts of argon recoil. Sample 1132B with a plateau age of 86.7 ± 1.1 (1.3) Ma is therefore considered to be geologically significant and all samples are of the same age.

The closure temperature of muscovite for Sr diffusion is estimated to be ~500 ± 50 °C and for Ar

diffusion between 350 and 500 °C (Purdy & Jäger, 1976; Cliff, 1985; Villa, 1998; Sherlock *et al.*, 1999). As the phengite separates were not pure, the age values cannot be considered as real phengite-whole Rb–Sr and phengite $^{40}\text{Ar}/^{39}\text{Ar}$ ages. In any case, the highest metamorphic temperatures experienced by these blueschists (~300 °C) are lower than the ‘assumed’ closure temperatures. The consistency of $^{40}\text{Ar}/^{39}\text{Ar}$ and Rb–Sr ages rules out the existence of excess argon, which is an important problem in high- P / T metamorphic rocks (e.g. Arnaud & Kelley, 1995; Scaillet, 1996; Sherlock *et al.*, 1999; Giorgis *et al.*, 2000; El-Shazly *et al.*, 2001), and indicates that the age of high- P /low- T metamorphism (87–85 Ma) is at the Coniacian/Santonian boundary (Ogg *et al.*, 2004).

DISCUSSION

Implications for the exhumation

Petroleum exploration wells drilled in southern Thrace (Ortaköy-1, Şarköy-1, Araplı-1) to the south of the Ganos Fault systematically cut through Miocene fluviatile to lagoonal sediments, olistostromal Eocene sequences and Upper Eocene limestone, and enter an ophiolitic basement similar to that exposed in the Sarıkaya tectonic sliver and found as olistoliths in the Upper Eocene clastics (e.g. Alaygut, 1996; Yalçınrak, 1996; Yazman, 1997). This indicates that the basement of southern Thrace to the south of the Ganos Fault is made up of an oceanic accretionary complex that must have been forming during Late Cretaceous to Palaeocene time. This is shown by the age of the blueschists (Coniacian/Santonian) and that of the pelagic limestone olistoliths.

Table 7. Ar–Ar data for the phengite concentrates from a blueschist (1132B) and a metachert (1131/1 & 1131/2) from the Şarköy area.

Step	T (°C)	⁴⁰ Ar* (10 ⁻⁶ cm ³ STP/g)	⁴⁰ Ar* (%)	³⁷ Ar/ ³⁹ Ar	⁴⁰ Ar*/ ³⁹ Ar	³⁹ Ar degassing (%)	Age (Ma)
<i>1132B Phengite (J value 16.33 ± 0.04 × 10⁻⁴), K = 5.6 wt%</i>							
1	400	0.019 ± 0.010	3.9 ± 1.9	0.42 ± 0.04	6.1 ± 3.0	0.48	17.8 ± 8.8 (8.8)
2	500	0.335 ± 0.030	61.8 ± 5.6	1.21 ± 0.06	20.6 ± 1.9	2.54	59.7 ± 5.3 (5.4)
3	550	0.706 ± 0.024	79.1 ± 2.8	3.38 ± 0.14	27.4 ± 1.0	4.01	79.0 ± 2.8 (2.8)
4	590	1.165 ± 0.016	40.4 ± 1.2	2.18 ± 0.08	29.98 ± 0.84	6.06	86.2 ± 2.4 (2.5)
5	630	2.870 ± 0.042	32.5 ± 0.5	2.31 ± 0.10	30.07 ± 0.44	14.88	86.5 ± 1.3 (1.4)
6	670	3.070 ± 0.020	92.7 ± 0.6	0.072 ± 0.003	29.94 ± 0.22	15.99	86.1 ± 0.7 (0.9)
7	700	2.975 ± 0.026	94.9 ± 1.0	0.0293 ± 0.0012	30.18 ± 0.30	15.37	86.8 ± 0.9 (1.1)
8	730	3.336 ± 0.040	97.0 ± 1.2	0.0219 ± 0.0012	30.39 ± 0.44	17.12	87.4 ± 1.3 (1.4)
9	760	3.142 ± 0.012	96.2 ± 0.4	0.0259 ± 0.0010	30.27 ± 0.14	16.18	87.1 ± 0.4 (0.7)
10	790	0.956 ± 0.014	85.9 ± 1.3	0.061 ± 0.009	29.76 ± 0.48	5.01	85.6 ± 1.4 (1.5)
11	850	0.371 ± 0.022	88.8 ± 5.4	0.302 ± 0.016	30.2 ± 1.9	1.92	86.7 ± 5.3 (5.3)
12	1100	0.068 ± 0.006	27.1 ± 2.6	13.78 ± 0.66	25.2 ± 2.5	0.42	72.7 ± 7.0 (7.0)
Total		19.01 ± 0.09	66.56 ± 0.34	0.74 ± 0.04	29.65 ± 0.36	100.00	85.3 ± 1.0 (1.2)
<i>1131/1 Phengite (J value 16.27 ± 0.08 × 10⁻⁴), K = 2.1 wt%</i>							
1	400	0.051 ± 0.022	10.3 ± 4.7	0.018 ± 0.008	10.1 ± 4.6	2.09	29 ± 13 (13)
2	500	0.596 ± 0.016	82.7 ± 2.1	0.0066 ± 0.0036	22.52 ± 0.58	11.04	64.9 ± 1.7 (1.7)
3	550	1.118 ± 0.024	91.5 ± 1.9	0.0102 ± 0.0032	28.83 ± 0.62	16.19	82.7 ± 1.8 (1.9)
4	600	1.610 ± 0.042	96.1 ± 2.5	0.0042 ± 0.0020	30.75 ± 0.82	21.85	88.1 ± 2.3 (2.4)
5	650	1.391 ± 0.034	97.2 ± 2.3	0	31.37 ± 0.76	18.52	89.8 ± 2.2 (2.3)
6	700	1.324 ± 0.028	96.1 ± 2.0	0	31.12 ± 0.64	17.76	89.1 ± 1.9 (2.0)
7	750	0.559 ± 0.014	88.3 ± 2.1	0.0165 ± 0.0030	30.68 ± 0.74	7.61	87.9 ± 2.1 (2.2)
8	820	0.245 ± 0.020	71.3 ± 6.1	0.062 ± 0.012	28.2 ± 2.4	3.62	81.0 ± 6.8 (6.8)
9	1200	0.119 ± 0.034	36 ± 10	0.350 ± 0.026	38 ± 11	1.32	107 ± 29 (29)
Total		7.01 ± 0.08	85.3 ± 1.0	0.0118 ± 0.0012	29.27 ± 0.50	100.00	83.9 ± 1.4 (1.6)
<i>1131/2 Phengite (J value 16.37 ± 0.03 × 10⁻⁴), K = 3.2 wt%</i>							
1	400	0.02 ± 0.11	2 ± 10	0.056 ± 0.024	7 ± 34	1.40	21 ± 98 (98)
2	500	0.431 ± 0.046	50.2 ± 5.2	0.177 ± 0.012	21.9 ± 2.3	8.16	63.6 ± 6.7 (6.7)
3	600	1.847 ± 0.074	79.1 ± 3.2	0.273 ± 0.012	29.3 ± 1.2	26.15	84.5 ± 3.4 (3.4)
4	680	2.776 ± 0.084	78.5 ± 2.4	0.0084 ± 0.0022	31.3 ± 0.9	36.75	90.3 ± 2.6 (2.8)
5	760	1.596 ± 0.042	84.1 ± 2.2	0.0056 ± 0.0032	32.4 ± 0.8	20.47	93.1 ± 2.4 (2.6)
6	820	0.480 ± 0.050	64.8 ± 6.6	0.051 ± 0.006	34.6 ± 3.5	5.75	99 ± 10 (10)
7	900	0.038 ± 0.064	7 ± 13	0.11 ± 0.06	17 ± 28	0.95	48 ± 81 (81)
8	1100	-0.074 ± 0.054	-11 ± 8	1.3 ± 1.6	-180 ± 116	0.38	-255 ± 400 (400)
Total		7.12 ± 0.20	60.9 ± 1.7	0.100 ± 0.006	29.5 ± 0.9	100.00	85.2 ± 2.6 (2.7)

Uncertainties are ± 2σ; K is estimated from the amount of ³⁹Ar of the standard and the sample. Errors in parentheses comprise age error and uncertainty of standard. The in-house standard 'Bmus/2' (Bärhalde muscovite) was used; age is 328.5 ± 2.2 Ma (2σ). ⁴⁰Ar* stands for radiogenic ⁴⁰Ar.

Table 8. Rb–Sr isotopic data for a blueschist (1132B) and a metachert (1131) from the Şarköy blueschist facies rocks, NW Turkey.

Sample	Rb (ppm)	Sr (ppm)	⁸⁷ Rb/ ⁸⁶ Sr ^a	⁸⁷ Sr/ ⁸⁶ Sr ^b	Age (Ma)
1132b (WR)	52.03	176.1	0.8548	0.705944 ± 0.09	
1132b (Phe)	143.0	165.3	2.5031	0.707970 ± 0.10	86.5 ± 1.8
1131 (WR)	43.01	74.49	1.6706	0.707728 ± 0.09	
1131 (Phe)	111.6	34.43	9.3891	0.717149 ± 0.09	85.9 ± 1.1

WR, whole rock; Phe, phengite.

^a2σ error equals 1%.

^b2σ error equals 0.003%.

The mineral assemblages in the blueschists and metadiabases are well preserved, and were not overprinted by any sub-greenschist or greenschist facies mineral assemblages, suggesting that they were not heated and/or subjected to fluid influx during the exhumation. The youngest non-metamorphic rocks that lie unconformably over the Sarıkaya serpentinite are Priabonian (Late Eocene) reefal limestones (Özcan *et al.*, 2006; E. Özcan, pers. comm.). These field relations suggest that the blueschist facies basement were at the Earth's surface during Late Eocene. There is a *c.* 47 Myr time lag between the blueschist facies

metamorphism (87–85 Ma) and sedimentation of the Late Eocene limestones (*c.* 38 Ma). Both the blueschist facies basement and overlying reefal limestones must have formed local topographic highs, providing olistoliths into the basin.

Exposures of blueschist belts along transpressional strike–slip fault zones are common in the circum-Pacific and the northern Caribbean (e.g. Mann & Gordon, 1996 and the references therein; Goncalves *et al.*, 2000). The North Anatolian Fault is thought to have formed in late Miocene (e.g. Şengör *et al.*, 2005) or Oligocene (e.g. Zattin *et al.*, 2005; Uysal *et al.*, 2006), therefore post-date the exhumation of the blueschist facies rocks. The present outcrop distribution and the post-Miocene exhumation (at least 1.8 to 2 km) of the blueschists are related to the transpressional strike–slip system but not their primary exhumation.

Geodynamic implications

Eclogite facies metamorphic rocks and Upper Cretaceous accretionary complexes are exposed throughout the Biga Peninsula (Fig. 1). The accretionary

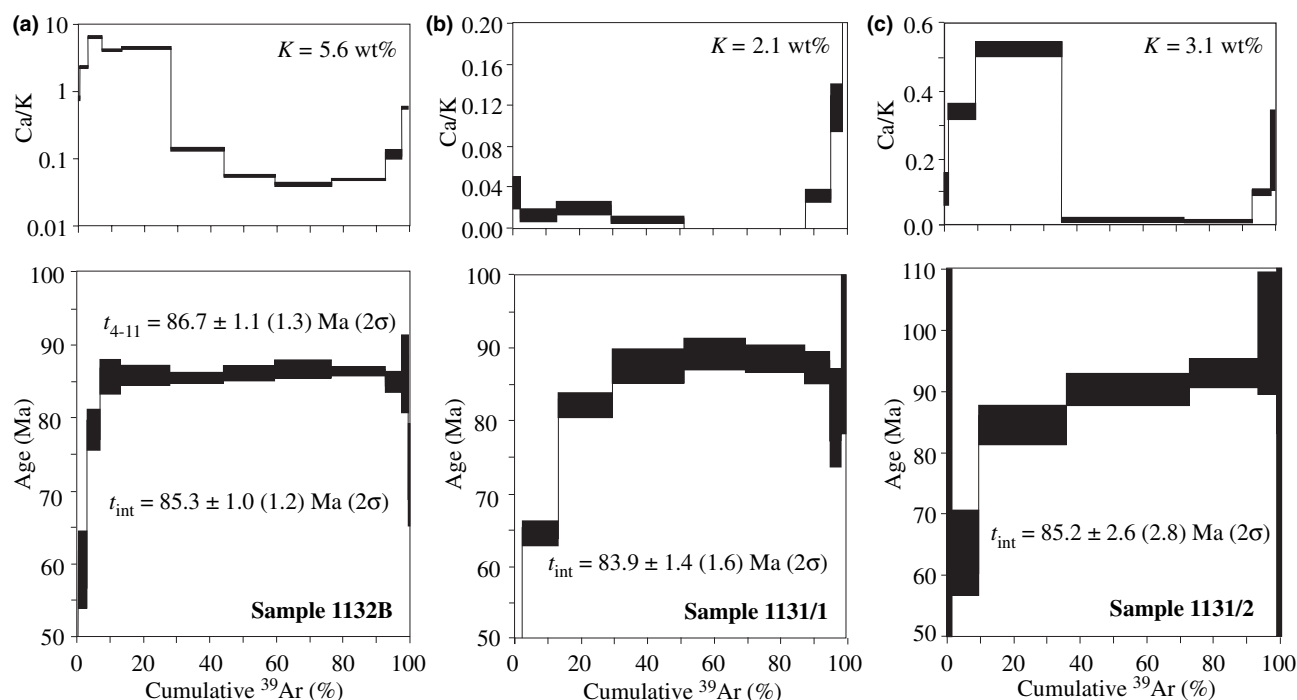


Fig. 11. ^{40}Ar – ^{39}Ar release spectra of phengite-rich separates from a blueschist sample (1132B) and from two aliquots of metachert (1131).

complexes comprise exotic tectonic blocks of eclogite. Other eclogite facies metamorphic rocks consist of quartz micaschists with minor calc-schist, marble, quartzite and metabasite. The metabasites locally preserve an early eclogite facies mineral assemblage of garnet + omphacite + glaucophane + rutile ± paragonite, strongly overprinted by greenschist facies mineral assemblages. The available age data on eclogites and other high- P/T rocks from the Biga peninsula range from 100 to 65 Ma, suggesting that subduction, accretion and underplating occurred over a relatively large time span (Okay & Satır, 2000a,b; Beccaletto & Jenny, 2004; Beccaletto *et al.*, 2007). Similarly, geochronological data from the Franciscan complex have revealed that the high-pressure metamorphism took place over a time span of over 75 Myr (e.g. Wakabayashi, 1999). Taken together, the data on the blueschists from southern Thrace (this paper) and the high- P/T rocks from the Biga peninsula (Okay & Satır, 2000a,b) suggest that Late Cretaceous represents a time period of continental growth through accretion in this part of the Mediterranean orogen.

Both southern Thrace and the Biga Peninsula lie to the SE of the Circum Rhodope Belt, which lies tectonically on the Rhodope Massif. This Circum Rhodope Belt comprises mainly greenschist facies rocks with local serpentinite and metagabbro (Magganas *et al.*, 1991; Magganas, 2002; Bonev & Stampfli, 2003, 2008) with Upper Jurassic ^{40}Ar – ^{39}Ar ages (Bonev *et al.*, 2008). Undated blueschist facies assem-

blages have also been reported (Michard *et al.*, 1994). The data from the Şarköy blueschists (this paper) and those from the Biga peninsula clearly demonstrate that active subduction and substantial accretionary crustal growth continued during Late Cretaceous time. The P – T conditions of these metamorphic areas are, however, highly different, ranging from ultrahigh-pressure conditions in the Rhodope Massif to greenschist–local blueschist facies conditions in the Circum Rhodope Belt and to the blueschist/eclogite facies in southern Thrace and on Biga Peninsula.

Late Cretaceous blueschist facies metamorphism is widespread throughout Turkey, e.g. in the Tavşanlı Zone and in the Central Pontides (e.g. Sherlock *et al.*, 1999; Davis & Whitney, 2006, 2008; Okay *et al.*, 2006). However, a direct correlation is not justified due to the occurrence of unrelated distinct crustal fragments. The presence of high-pressure metamorphics in different tectonic zones should be related to concurrent subduction–accretion events related to the consumption of the different branches of the Neotethys (e.g. Şengör & Yılmaz, 1981; Okay & Tüysüz, 1999).

CONCLUSIONS

The pre-Eocene basement of southern Thrace is made up of a very low-grade blueschist facies accretionary complex, which is exposed in an uplifted tectonic sliver bounded by the strands of the Ganos strike slip fault. Blueschist facies metamorphism

occurred during the Late Cretaceous (87–85 Ma, Coniacian/Santonian) at a depth of 23–29 km and temperatures of 270–350 °C. During late Eocene, this blueschist facies basement was exhumed and formed local topographic highs providing olistoliths into flyschoid sequences. Post-Miocene exhumation of the blueschists occurred along a transpressional segment of the North Anatolian Fault. Together with the diverse high-*P/T* rocks of the Biga Peninsula (100–65 Ma), the blueschist facies rocks from southern Thrace document a Late Cretaceous accretionary phase to the southeast of the older Circum Rhodope Belt.

ACKNOWLEDGEMENTS

We thank M. A. Oral and Y. Ilgar for cutting the rock slices, I. Fin and O. Wienand for preparing excellent polished thin sections, H.-P. Meyer and A. Varychev for assistance during EPMA and SEM work, G. Bartholoma for mineral separation, E. Reitter for Rb–Sr dating and I. Ece for XRD determinations. Travel and logistic expenses were covered by the TÜBITAK project #104Y155 and by the Turkish Academy of Sciences (TÜBA) with a grant to A. I. Okay. Discussions with C. Yaltrak on the geology of Turkish Thrace are gratefully appreciated. The constructive reviews of D. Whitney, T. Tsujimori and an anonymous referee helped to improve the manuscript considerably.

REFERENCES

- Alaygut, D., 1996. *Trakya Havzası'nın Temelindeki Kristalin Kayaların Mineralojik-Petrografik İncelenmesi*. Türkiye Petrolleri Anonim Ortaklığı (Turkish Petroleum Corporation), Ankara, Report 2140, 70 p.
- Aldanmaz, E., Köprübaşı, N., Gürer, Ö. F., Kaymakçı, N. & Gourgaud, A., 2006. Geochemical constraints on the Cenozoic, OIB-type alkaline volcanic rocks of NW Turkey: implications for mantle sources and melting processes. *Lithos*, **86**, 50–76.
- Anczkiewicz, R., Platt, J. P., Thirlwall, M. F. & Wakabayashi, J., 2004. Franciscan subduction off to a slow start: evidence from high-precision Lu–Hf garnet ages on high-grade blocks. *Earth and Planetary Science Letters*, **225**, 147–161.
- Arnaud, N. O. & Kelley, S. P., 1995. Evidence for excess argon during high-pressure metamorphism in the Dora Maira Massif (western Alps, Italy), using an ultra-violet laser ablation microprobe $^{40}\text{Ar}/^{39}\text{Ar}$ technique. *Contributions to Mineralogy and Petrology*, **121**, 1–11.
- Bauer, C., Rubatto, D., Krenn, K., Proyer, A. & Hoinkes, G., 2007. A zircon study from the Rhodope metamorphic complex, N-Greece: time record of a multistage evolution. *Lithos*, **99**, 207–228.
- Beccaletto, L. & Jenny, C., 2004. Geology and correlation of the Ezine zone: a Rhodope fragment in Turkey? *Turkish Journal of Earth Sciences*, **13**, 145–176.
- Beccaletto, L., Bonev, N., Bosch, D. & Bruguier, O., 2007. Record of a Paleogene syn-collisional extension in the north Aegean region: evidence from the Kemer micaschists (NW Turkey). *Geological Magazine*, **144**, 393–400.
- Bonev, N. G. & Stampfli, G. M., 2003. New structural and petrologic data on Mesozoic schists in the Rhodope (Bulgaria): geodynamic implications. *Comptes Rendues Geoscience*, **335**, 691–699.
- Bonev, N. & Stampfli, G., 2008. Petrology, geochemistry and geodynamic implications of Jurassic island arc magmatism as revealed by mafic volcanic rocks in the Mesozoic low-grade sequence, eastern Rhodope, Bulgaria. *Lithos*, **100**, 210–233.
- Bonev, N., Marchev, P. & Singer, B., 2006. $^{40}\text{Ar}/^{39}\text{Ar}$ geochronology constraints on the Middle Tertiary basement extensional exhumation, and its relation to ore-forming and magmatic processes in the Eastern Rhodope (Bulgaria). *Geodinamica Acta*, **19**, 265–280.
- Bonev, N., Spikings, R., Moritz, R. & Marchev, P., 2008. Structural and $^{40}\text{Ar}/^{39}\text{Ar}$ age constraints on the Kulidjik nappe: a record of an early Alpine thrust tectonics in the northeastern Rhodope Massif. *Symposium on the Geology of the Aegean*, University of Texas at Austin, Bulgaria, 28–30 April.
- Brady, J. B., Markley, M. J., Schumacher, J. C., Cheney, J. T. & Bianciardi, G. A., 2004. Aragonite pseudomorphs in high-pressure marbles of Syros, Greece. *Journal of Structural Geology*, **26**, 3–9.
- Bucher, K. & Frey, M., 2002. *Petrogenesis of Metamorphic Rocks, 7th completely revised and updated edition*. Springer, Berlin, Heidelberg, NY, 341 pp.
- Burg, J. P., Ricou, L. E., Ivanov, Z., Godfriaux, I., Dimov, D. & Klain, L., 1996. Syn-metamorphic nappe complex in the Rhodope Massif: structure and kinematics. *Terra Nova*, **8**, 6–15.
- Carpenter, M. A., 1980. Mechanisms of exsolution in sodic pyroxenes. *American Mineralogist*, **64**, 102–108.
- Cliff, R. A., 1985. Isotopic dating in metamorphic belts. *Journal of the Geological Society of London*, **142**, 97–110.
- Davis, P. B. & Whitney, D. L., 2006. Petrogenesis of lawsonite and epidote eclogite and blueschist, Sivrihisar Massif, Turkey. *Journal of Metamorphic Geology*, **24**, 823–849.
- Davis, P. B. & Whitney, D. L., 2008. Petrogenesis and structural petrology of high-pressure metabasalt pods, Sivrihisar, Turkey. *Contributions to Mineralogy and Petrology*, **156**, 217–241.
- El-Shazly, A. K., 1994. Petrology of lawsonite-, pumpellyite- and sodic amphibole-bearing metabasites from north-east Oman. *Journal of Metamorphic Geology*, **12**, 23–48.
- El-Shazly, A. K., Bröcker, M., Hacker, B. & Calvert, A., 2001. Formation and exhumation of blueschists and eclogites from NE Oman: new perspectives from Rb–Sr and $^{40}\text{Ar}/^{39}\text{Ar}$ dating. *Journal of Metamorphic Geology*, **19**, 233–248.
- Ercan, T., 1992. Trakya'daki Senozoyik volkanizması ve bölgesel yayılımı. *Jeoloji Mühendisliği*, **41**, 37–50.
- Ernst, W. G., 1979. Coexisting sodic and calcic amphiboles from high-pressure metamorphic belts and the stability of barroisitic amphibole. *Mineralogical Magazine*, **43**, 269–278.
- Evans, B. W., 1990. Phase relations of epidote blueschists. *Lithos*, **25**, 3–23.
- Frey, M., De Capitani, C. & Liou, J. G., 1991. A new petrogenetic grid for low-grade metabasites. *Journal of Metamorphic Geology*, **9**, 497–509.
- Giorgis, D., Cosca, M. & Li, S., 2000. Distribution and significance of extraneous argon in UHP eclogite (Sulu terrain, China): insight from in situ $^{40}\text{Ar}/^{39}\text{Ar}$ UV-laser ablation analysis. *Earth and Planetary Science Letters*, **181**, 605–615.
- Goncalves, P., Guillot, S., Lardeaux, J.-M., Nicollet, C. & de Lepinay, B. M., 2000. Thrusting and sinistral wrenching in a pre-Eocene HP-LT Caribbean accretionary wedge (Samaná Peninsula, Dominican Republic). *Geodinamica Acta*, **13**, 119–132.
- Goodge, J. W., 1995. Pre-Middle Jurassic accretionary metamorphism in the southern Klamath Mountains of northern California, USA. *Journal of Metamorphic Geology*, **13**, 93–110.
- Goodge, J. W. & Renne, P. R., 1993. Middle-Paleozoic olistoliths in the Eastern Hayfork Terrane mélange, Klamath Mountains: implications for late-Paleozoic – Early Mesozoic Cordilleran forearc development. *Tectonics*, **12**, 279–289.
- Görür, N. & Okay, A. I., 1996. Fore-arc origin of the Thrace basin, northwest Turkey. *International Journal of Earth Sciences (Geologische Rundschau)*, **85**, 662–668.

- Green, E., Holland, T. & Powell, R., 2007. An order-disorder model for omphacitic pyroxenes in the system jadeite-diopside-hedenbergite-acmite, with applications to eclogitic rocks. *American Mineralogist*, **92**, 1181–1189.
- Hatert, F., Pasero, M., Perchiazzi, N. & Theye, T., 2007. Pumpellyite-(Al), a new mineral from Bertrix, Belgian Ardennes. *European Journal of Mineralogy*, **19**, 247–253.
- Himmelberg, G. R. & Papike, J. J., 1969. Coexisting amphiboles from blueschist facies metamorphic rocks. *Journal of Petrology*, **10**, 102–114.
- Holland, T. J. B., 1983. The experimental determination of activities in disordered and short-range ordered jadeitic pyroxenes. *Contributions to Mineralogy and Petrology*, **82**, 214–220.
- Kauffmann, G., Kockel, F. & Mollat, H., 1976. Notes on the stratigraphic and paleogeographic position of the Svoula Formation in the innermost zone of the Hellenides (Northern Greece). *Bulletin de la Société géologique de France*, **18**, 29–34.
- Kopp, K.-O., Pavoni, N. & Schindler, C., 1969. Geologie Thrakiens IV: Das Ergene-Becken. *Beihefte zum Geologisches Jahrbuch*, **76**, 171.
- Krogh, E. J., Oh, C. W. & Liou, J. G., 1994. Polyphase and anticlockwise *P-T* evolution for Franciscan eclogites and blueschists from Jenner, California, USA. *Journal of Metamorphic Geology*, **12**, 121–134.
- Leake, B. E., Woolley, A. R. & Arps, C. E. S. *et al.*, 1997. Nomenclature of amphiboles: report of subcommittee on amphiboles of the international mineralogical association commission on new minerals and mineral names. *European Journal of Mineralogy*, **9**, 623–651.
- Liati, A., 2005. Identification of repeated Alpine (ultra) high-pressure metamorphic events by U-Pb SHRIMP geochronology and REE geochemistry of zircon: the Rhodope zone of Northern Greece. *Contributions to Mineralogy and Petrology*, **150**, 608–630.
- Liati, A. & Gebauer, D., 1999. Constraining the prograde and retrograde *P-T-t* path of Eocene HP rocks by SHRIMP dating of different zircon domains: inferred rates of heating, burial, cooling and exhumation for central Rhodope, northern Greece. *Contributions to Mineralogy and Petrology*, **135**, 340–354.
- Liati, A. & Mposkos, E., 1990. Evolution of the eclogites in the Rhodope Zone of northern Greece. *Lithos*, **25**, 89–99.
- Liati, A. & Seidel, E., 1996. Metamorphic evolution and geochemistry of kyanite eclogites in central Rhodope, northern Greece. *Contributions to Mineralogy and Petrology*, **123**, 293–307.
- Liati, A., Gebauer, D. & Wysoczanski, R., 2002. U-Pb SHRIMP dating of zircon domains from UHP garnet-rich mafic rocks and late pegmatoids in the Rhodope zone (N Greece): evidence for Early Cretaceous crystallization and Late Cretaceous metamorphism. *Chemical Geology*, **184**, 281–299.
- Liou, J. G. & Maruyama, S., 1987. Parageneses and compositions of amphiboles from Franciscan jadeite glaucophane type facies series metabasites at Cazadero, California. *Journal of Metamorphic Geology*, **5**, 371–395.
- Liou, J. G., Maruyama, S. & Cho, M., 1985. Phase equilibria and mineral paragenesis of metabasites in low-grade metamorphism. *Mineralogical Magazine*, **49**, 321–333.
- Liou, J. G., Maruyama, S. & Cho, M., 1987. Very low-grade metamorphism of volcanic and volcanoclastic rocks – mineral assemblages and mineral facies. In: *Low Temperature Metamorphism* (ed. Frey, M.), pp. 59–113. Blackie, Glasgow.
- Magganas, A. C., 2002. Constraints on the petrogenesis of Evros ophiolite extrusives, NE Greece. *Lithos*, **65**, 165–182.
- Magganas, A., Sideris, C. & Kokkinakis, A., 1991. Marginal basin-volcanic arc origin of metabasic rocks of the Circum-Rhodope Belt, Thrace, Greece. *Mineralogy and Petrology*, **44**, 235–252.
- Mann, P. & Gordon, M. B., 1996. Tectonic uplift and exhumation of blueschist belts along transpressional strike-slip fault zones. In: *Subduction Top to Bottom* (eds Bebout, G.E., Scholl, D.W., Kirby, S.H. & Platt, J.P.), *AGU Geophysical Monograph*, **96**, 143–154.
- Marimoto, N., Fabriès, J., Ferguson, A. K. *et al.*, 1988. Nomenclature of pyroxenes. *American Mineralogist*, **73**, 1123–1133.
- Maruyama, S., Cho, M. & Liou, J. G., 1986. Experimental investigations of blueschist-greenschist transition equilibria: Pressure dependence of Al₂O₃ contents in sodic amphiboles – A new geobarometer. In: *Blueschists and Eclogites* (eds Evans, B.W. & Brown, E.H.), *Geological Society of America Memoir*, **164**, 1–16.
- Maruyama, S. & Liou, J. G., 1985. The stability of Ca-Na pyroxene in low-grade metabasites of high-pressure intermediate facies series. *American Mineralogist*, **70**, 16–29.
- Maruyama, S. & Liou, J. G., 1988. Petrology of Franciscan metabasites along the jadeite-glaucophane type facies series, Cazadero, California. *Journal of Petrology*, **29**, 1–37.
- Maruyama, S., Liou, J. G. & Terabayashi, M., 1996. Blueschists and eclogites of the world and their exhumation. *International Geology Review*, **38**, 485–594.
- Matsumoto, K. & Hirajima, T., 2005. The coexistence of jadeite and omphacite in an eclogite-facies metaquartz diorite from the southern Sessia Zone, Western Alps, Italy. *Journal of Mineralogical and Petrological Sciences*, **100**, 70–84.
- Michard, A., Goffé, B., Liati, A. & Mountrakis, D., 1994. Découverte du faciès schiste bleu dans les nappes du Circum-Rhodope: un élément d'une ceinture HP-BT éohellénique en Grèce septentrionale? *Comptes Rendues Académie Sciences Paris, Série II*, **318**, 1535–1542.
- Moore, D., 1984. Metamorphic history of a high-grade blueschist exotic block from the Franciscan Complex, California. *Journal of Petrology*, **25**, 126–150.
- Mposkos, E. & Kostopoulos, D., 2001. Diamond, former coesite and supersilicic garnet in metasedimentary rocks from the Greek Rhodope: a new ultrahigh-pressure metamorphic province established. *Earth and Planetary Science Letters*, **192**, 497–506.
- Mposkos, E. & Krohe, A., 2006. Pressure-temperature-deformation paths of closely associated ultra-high-pressure (diamond-bearing) crustal and mantle rocks of the Kimi complex: implications for the tectonic history of the Rhodope Mountains, northern Greece. *Canadian Journal of Earth Sciences*, **43**, 1755–1776.
- O'Hanley, D. S., 1996. *Serpentinites: Records of Tectonic and Petrological History*, 1st edn. Oxford University Press, New York, Oxford, 277 pp.
- Ogg, J. G., Agterberg, F. P. & Gradstein, F. M., 2004. The Cretaceous period. In: *A Geologic Time Scale 2004* (eds Gradstein, F.M., Ogg, J.G. & Smith, A.G.), pp. 344–383. Cambridge University Press, Cambridge, UK.
- Okay, A. I., 1980. Mineralogy, petrology and phase relations of glaucophane-lawsonite zone blueschists from the Tavşanlı region, northwest Turkey. *Contributions to Mineralogy and Petrology*, **72**, 243–255.
- Okay, A. I., 1982. Incipient blueschist metamorphism and metasomatism in the Tavşanlı region, northwest Turkey. *Contributions to Mineralogy and Petrology*, **79**, 361–367.
- Okay, A. I. & Satır, M., 2000a. Coeval plutonism and metamorphism in a latest Oligocene metamorphic core complex in northwest Turkey. *Geological Magazine*, **137**, 495–516.
- Okay, A. I. & Satır, M., 2000b. Upper Cretaceous eclogite-facies metamorphic rocks from the Biga Peninsula, northwest Turkey. *Turkish Journal of Earth Sciences*, **9**, 47–56.
- Okay, A. I. & Tansel, I., 1992. New data on the upper age of the Intra-Pontide ocean from north of Sarköy (Thrace). *Bulletin of Mineral Research and Exploration*, **114**, 23–26.
- Okay, A. I. & Tüysüz, O., 1999. Tethyan sutures of northern Turkey. In: *The Mediterranean Basins: Tertiary Extension within the Alpine Orogen* (eds Durand, B., Jolivet, L., Horváth, F. & Séranne, M.), *Geological Society London Special Publication*, **156**, pp. 475–515.

- Okay, A. I., Harris, N. B. W. & Kelley, S. P., 1998. Exhumation of blueschists along a Tethyan suture in northwest Turkey. *Tectonophysics*, **285**, 275–299.
- Okay, A. I., Demirbağ, E., Kurt, H., Okay, N. & Kuşçu, I., 1999. An active deep marine strike-slip basin along the North Anatolian fault in Turkey. *Tectonics*, **18**, 129–147.
- Okay, A. I., Satır, M., Tüysüz, O., Akyüz, S. & Chen, F., 2001. The tectonics of the Strandja Massif: Late Variscan and mid-Mesozoic deformation and metamorphism in the northern Aegean. *International Journal of Earth Sciences (Geologische Rundschau)*, **90**, 217–233.
- Okay, A. I., Tüysüz, O., Satır, M. *et al.*, 2006. Cretaceous and Triassic subduction-accretion, HP/LT metamorphism and continental growth in the Central Pontides, Turkey. *Geological Society of America Bulletin*, **118**, 1247–1269.
- Özbek, O. & Erol, K., 2001. Étude pétrographique de haches polies de Hamaylıtarla et Fenerkaradutlar (Turquie). *Anatolia Antiqua*, **IX**, 1–7.
- Özcan, E., Less, G., Báldi-Beke, M., Kollányi, K. & Kertész, B., 2006. Biometric analysis of middle and upper Eocene Discocyclinidae and Orbitoclypeidae (Foraminifera) from Turkey and updated orthophragmine zonation in the Western Tethys. *Micropaleontology*, **52**, 485–520.
- Pouchou, J. L. & Pichoir, F., 1984. A new model for quantitative analyses. I. Application to the analysis of homogeneous samples. *La Recherche Aérospatiale*, **3**, 13–38.
- Pouchou, J. L. & Pichoir, F., 1985. PAP[®] (f-r-Z) correction procedure for improved quantitative microanalysis. In: *Microbeam Analysis* (ed. Armstrong, J.T.), pp. 104–106. San Francisco Press, San Francisco, CA.
- Purdy, J. W. & Jäger, E., 1976. K-Ar ages on rock forming minerals from the Central Alps. *Institute of Geology and Mineralogy Padova University Memoirs*, **30**, 1–30.
- Reynard, B. & Ballèvre, M., 1988. Coexisting amphiboles in the eclogite from the Western Alps: new constraints on the miscibility gap between sodic and calcic amphiboles. *Journal of Metamorphic Geology*, **6**, 333–350.
- Ricou, L.-E., Burg, J.-P., Godfriaux, I. & Ivanov, Z., 1998. Rhodope and Vardar: the metamorphic and the olistostromic paired belts related to the Cretaceous subduction under Europe. *Geodinamica Acta*, **11**, 285–309.
- Scaillet, S., 1996. Excess ⁴⁰Ar transport scale and mechanism in high-pressure phengites: a case study from an eclogitized metabasite of the Dora-Maira nappe, Western Alps. *Geochimica et Cosmochimica Acta*, **60**, 1075–1090.
- Schiffman, P. & Day, H. W., 1999. Petrological methods for the study of very low-grade metabasites. In: *Low-Grade Metamorphism* (eds Frey, M. & Robinson, D.), 313 pp. Blackwell Science Ltd., Oxford, London.
- Schwarz, W. H. & Trieloff, M., 2007. Intercalibration of ⁴⁰Ar-³⁹Ar age standards NL-25, HB3gr hornblende, GA1550, SB-3, HD-B1 biotite and Bmus/2 muscovite. *Chemical Geology*, **242**, 218–231.
- Şengör, A. M. C. & Yılmaz, Y., 1981. Tethyan evolution of Turkey: a plate tectonic approach. *Tectonophysics*, **75**, 181–241.
- Şengör, A. M. C., Tüysüz, O., İmren, C. *et al.*, 2005. The North Anatolian fault: a new look. *Annual Review of Earth and Planetary Sciences*, **33**, 37–112.
- Sherlock, S., Kelley, S., Inger, S., Harris, N. & Okay, A. I., 1999. ⁴⁰Ar-³⁹Ar and Rb-Sr geochronology of high-pressure metamorphism and exhumation history of the Tavşanlı Zone, NW Turkey. *Contributions to Mineralogy and Petrology*, **137**, 46–58.
- Spaggiari, C. V., Gray, D. R. & Foster, D. A., 2002. Blueschist metamorphism during accretion in the Lachlan Orogen, south-eastern Australia. *Journal of Metamorphic Geology*, **20**, 711–726.
- Sunal, G., Natal'in, B., Satır, M. & Toroman, E., 2006. Paleozoic magmatic events in the Strandja Massif, NW Turkey. *Geodinamica Acta*, **19**, 283–300.
- Topuz, G. & Altherr, R., 2004. Pervasive rehydration of granulites during exhumation – an example from the Pulur complex, Eastern Pontides, Turkey. *Mineralogy and Petrology*, **81**, 165–185.
- Topuz, G., Okay, A. I., Altherr, R., Meyer, H.-P. & Nasdala, L., 2006. Partial high-pressure aragonitization of micritic limestones in an accretionary complex, Tavşanlı Zone, NW Turkey. *Journal of Metamorphic Geology*, **24**, 603–613.
- Topuz, G., Altherr, R., Schwarz, W. H., Dokuz, A. & Meyer, H.-P., 2007. Variscan amphibolite-facies rocks from the Kurtoğlu metamorphic complex (Gümüşhane area, Eastern Pontides, Turkey). *International Journal of Earth Sciences (Geologische Rundschau)*, **96**, 861–873.
- Tsujimori, T., 1997. Omphacite-diopside vein in an omphacite block from the Osayama serpentinite mélange, Sangun-Renge metamorphic belt, southwestern Japan. *Mineralogical Magazine*, **61**, 845–852.
- Tsujimori, T., Liou, J. G. & Coleman, R. G., 2005. Coexisting retrograde jadeite and omphacite in a jadeite-bearing lawsonite eclogite from the Motagua Fault Zone, Guatemala. *American Mineralogist*, **90**, 836–842.
- Tsujimori, T., Matsumoto, K., Wakabayashi, J. & Liou, J. G., 2006. Franciscan eclogite revisited: reevaluation of the P-T evolution of tectonic blocks from Tiburon Peninsula, California, U.S.A. *Mineralogy and Petrology*, **88**, 243–267.
- Turgut, S., Türkaslan, M. & Perinçek, D., 1991. Evolution of the Thrace sedimentary basin and its hydrocarbon prospectivity. In: *Generation, Accumulation and Production of Europe's Hydrocarbons* (ed. Spencer, A.M.), Special Publication of European Association of Petroleum Geoscientists, **1**, 415–437.
- Uysal, I. T., Mutlu, H., Altunel, E., Karabacak, V. & Golding, S. D., 2006. Clay mineralogical and isotopic (K-Ar, $\delta^{18}\text{O}$, δD) constraints on the evolution of the North Anatolian fault zone, Turkey. *Earth and Planetary Science Letters*, **243**, 181–194.
- van Hinsbergen, D. I. J., Hafkenscheid, E., Spakman, W., Meulenkamp, J. E. & Wortel, R., 2005. Nappe stacking resulting from subduction of oceanic and continental lithosphere below Greece. *Geology*, **33**, 325–328.
- Villa, I. M., 1998. Isotopic closure. *Terra Nova*, **10**, 42–47.
- Wakabayashi, J., 1990. Counterclockwise P-T-t paths from amphibolites, Franciscan Complex, California – relics from the early stages of subduction zone metamorphism. *Journal of Geology*, **98**, 657–680.
- Wakabayashi, J., 1999. Subduction and the rock record: concepts developed in the Franciscan Complex, California. In: *Classic Cordilleran Concepts: A View From California* (eds Sloan, D., Moores, E.M. & Stout, D.), *Geological Society of America Special Paper*, **338**, pp. 123–133.
- Yaltrak, C., 1996. Ganos Fay sisteminin tektonik tarihi. *Türkiye Petrol Jeologları Derneği Bülteni*, **8**, 137–156.
- Yazman, M., 1997. Kuzey Ege'nin jeolojisi ve petrol olanakları. Istanbul Technical University, Mining Faculty Colloquium, 26th June, Istanbul, Bildiri Özleri, **1**, 45–52.
- Zattin, M., Okay, A. I. & Cavazza, W., 2005. Fission-track evidence for late Oligocene and mid-Miocene activity along the North Anatolian Fault in south-western Thrace. *Terra Nova*, **17**, 95–101.
- Zhang, L., Sun, M. & Xu, B., 2001. Phase relations in garnet-bearing metabasites of prehnite-pumpellyite facies from the Darbut-Sartuohai ophiolite, Western Junggar of Xinjiang, China. *Mineralogy and Petrology*, **71**, 67–85.

Received 21 March 2008; revision accepted 1 September 2008.